# Interaction of a Monochromatic Ultrasonic Beam with a Finite Length Defect at the Interface Between Two Anisotropic Layers: Kirchhoff Approximation and Fourier Representation

Bruno Vacossin, Catherine Potel, Philippe Gatignol, and Jean-François de Belleval, *Member, IEEE*

***Abstract*—This paper presents a fast computation method to simulate the interaction between a bounded acoustic beam and a 2-layered anisotropic structure with a finite defect on the internal interface. The method uses the classical Fourier decomposition of the fields into plane waves, and the Kirchhoff approximation is introduced to calculate the diffusion by the defect. The validity of the approximation is estimated by comparison with the Keller Geometrical Theory of Diffraction and with results obtained by boundary element methods. The quickness of the method allows testing several geometrical configurations (varying incident angle, thickness of the layers or the physical nature of the defect). These studies may be used to foresee what experimental configurations would be adequate to have a chance to detect the defect.**

## I. Introduction: The Problem

Various physical and geometrical parameters can influence the ability to detect a defect in immersed anisotropic structures, using ultrasonic nondestructive testing (NDT). Numerical simulations now play an important role [1], [2] and are widely used to conceive methods and demonstrate their performance. This paper aims to develop a rapid simulation method capable of performing parametric studies to determine the "good" testing configuration (frequency, incident angle), when complex structures (such as composite structures including a delamination defect or a weak bonding) are involved. The final aim is to integrate this simulation method in an industrial platform [1]. In this paper, the testing setup is assumed to be constituted both of a fixed oblique emitting transducer that can generate guided waves (such as Lamb waves) in the structure and of a receiver that can be moved parallel to the structure to measure the pressure amplitudes of the re-emitted field in the external fluid; the cases of a notable discrepancy between the field re-emitted by a healthy structure and that by a structure including a defect, are particularly of interest. Therefore, a parametrical study is carried out to examine the influence of the incident angle, the azimuthal orientation of the incident acoustic beam, the frequency, the location, and nature of the defect. Thus, the aim of the paper is, first, to present a fast simulation method using the Kirchhoff approximation to study the interaction of an acoustic bounded beam with an anisotropic composite structure including a finite-sized delamination defect, under high-frequency approximation, no far-field approximation being made. The second aim of the paper is then to show how this simulation technique is suitable to work out the circumstances that are favorable to a good detection of a defect.

The modeling of the propagation in anisotropic multilayered plane structures is now available and well known [3]–[6], even if many problems still exist when studying the propagation in healthy structures, for example, complex shapes and resin transfer molding (RTM). Taking into account an infinite-sized defect between 2 layers (bonding condition between 2 parallel interfaces) is also not a major problem [7]; the quality of the bonding can be then appreciated through the study of the reflection and transmission coefficients as a function of stiffness coefficients. The structures involved in the literature for this kind of modeling are either isotropic or anisotropic multilayered structures.

On the other hand, the modeling of a finite-sized defect is more complex (a useful review of the different methods used for detecting defects, notably in composite media, can be found in [2]) and often needs the use of the boundary element method (BEM). It needs at least approximations, such as the Kirchhoff approximation used by Spies [8] to model, in the far field, the interaction of elastic plane waves with an infinite anisotropic medium in which the defect consists of traction-free spheres embedded in the medium; the 3-D scattering is studied using, like many authors, Green's triadic function. The method has been validated for high frequencies and weak incident angles. In the same situation, for various defects, Huang *et al.* [9] and Schmerr [10] use the Kirchhoff approximation for plane waves and in the far field, thus validating Kirch-

Manuscript received August 3, 2008; accepted June 26, 2009.

B. Vacossin, P. Gatignol, and J.-F. de Belleval are with Université de Technologie de Compiègne—Laboratoire Roberval, UMR CNRS 6253,Compiègne, France.

B. Vacossin is also with Université de Picardie Jules Verne, IUT de l'Aisne-Qualité, Logistique Industrielle et Organisation, Soissons-Cuffies, France.

C. Potel is with Université du Maine—Laboratoire d'Acoustique de l'Université du Maine (LAUM, UMR CNRS 6613), Le Mans, France (e-mail: catherine.potel@univ-lemans.fr).

C. Potel is also with Fédération Acoustique du Nord-Ouest (FANO, FR CNRS 3110), France.

Digital Object Identifier 10.1109/TUFFC.2009.1307

0885–3010/$25.00 © 2009 IEEE

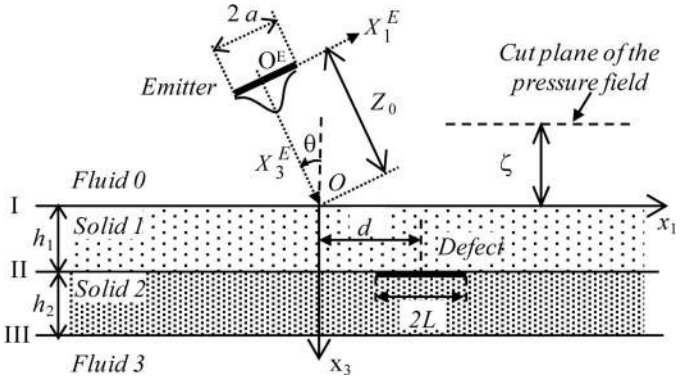


Fig. 1. Geometry of the problem.

TABLE I. Nomenclature of Subscripts and Superscripts.

| Notation | Meaning |
|---|---|
| Superscripts | |
| $(e)$ | Exact solution |
| $(i)$ | Infinite defect on interface II |
| $(h)$ | Healthy interface II |
| $(k)$ | Kirchhoff approximation |
| $(s)$ | Scattered field under the Kirchhoff approximation |
| $\alpha$ | Medium, $\alpha = 0,1,2,3$ |
| Subscripts | |
| $a$ | Waves propagating toward $x_3 > 0$ |
| $b$ | Waves propagating toward $x_3 < 0$ |
| $i$ | Component on $x_1$-axis |
| inc | Incident field (in fluid medium 0) |
| ref | Reflected field (in fluid medium 0) |
| tr | Transmitted field (in fluid medium 3) |

For example: $\mathbf{u}_b^{1(s)}$ = scattered field propagating toward $x_3 < 0$ in medium 1; $u_{3a}^{1(h)}$ = component on $x_3$ axis of the field $\mathbf{u}_a^{1(h)}$, i.e., the field propagating toward $x_3 > 0$ in medium 1 for a structure with a healthy surface II.

hoff approximation for this application. The comparison of the Kirchhoff approximation with the BEM has been performed by Foote and Francis [11] in the far field, in the case of acoustic back-scattering from fish. The defect (the fish swimbladder) is modeled by a void, the surface of which is represented by a mesh derived from measurements of microtomed sections, and the 2 models are independently validated. Notably, the accuracy of the results from the Kirchhoff approximation for high frequencies is preserved, in comparison with the BEM.

Another method, the ray method, can also be used (the pencil method [12] uses the calculation of energy in ray tubes): it is a high-frequency approximation of Fourier integrals. Croce *et al.* [13] use a method that seems close to the method described in the present paper, in the meaning that the ray technique disregards (as in the Kirchhoff approximation) a part of the scattering effects on the edges of a defect; however, this Croce's method is limited by the multiple reflections when there are too many interfaces. Another numerical method, the distributed point source method (DPSM), has been taken up (with 267 sources and matrices to invert) and compared with experimental results for multilayered structures by Banerjee and Kundu [14]. More precisely, inclusion or cavity-type defects in a single anisotropic layer have been detected using Lamb waves generated by an ultrasonic beam. The detection of microcrack initiation and evolution in a fatigue sample is also successfully experimentally performed using Lamb waves by Rokhlin *et al.* [15]. The authors also describe the propagation of acoustic waves in anisotropic multilayered structures. The case of the propagation of Lamb waves in viscoelastic materials is described by Hosten *et al.* [16]: results obtained via a finite element method (FEM) and a semi-analytic method are compared: the results are in good agreement, notably for the detection of a notch in a single layer.

All these papers bring significant contributions to the problem, but, to the authors' knowledge, none of them implements the Kirchhoff approximation in the area of multilayered anisotropic structures including finite-sized interface defects, for bounded beams, with no far-field hypothesis.

Thus, the aim of this paper is to study, using the Kirchhoff approximation, the interaction of a monochromatic ultrasonic bounded beam with a 2-layer anisotropic structure including a finite length defect and immersed in a fluid, and to obtain the reflected and transmitted fields (Fig. 1). The nomenclature used in this paper is defined in Table I. Fluid media 0 and 3 above and below the structure are semi-infinite (these fluid media are identical but have different numbers for convenience). The interface plane is denoted $(Ox_1x_2)$, the $x_3$-axis being perpendicular to the interfaces (denoted I, II, and III) and the acoustic axis of the emitting transducer (diameter $2a$, frequency $f = \omega/(2\pi)$) makes an angle $\theta$ with the $x_3$-axis. The structure is made up of 2 anisotropic layers 1 and 2 (thicknesses denoted $h_1$ and $h_2$) perfectly bonded all along their common interface II, except on a $2L$-length delamination-type defect. The geometry of the problem is a 2-D one, but the 3-D effects caused by the anisotropy are taken into account (in particular, the particle displacement and stress vectors may have 3 components).

## II. The Method of Solution, Using the Kirchhoff Approximation

We propose here to solve the problem of the interaction between an incident acoustic beam and a bilayered solid structure with a finite defect by the Kirchhoff approximation. In the scope of this study, the Kirchhoff approximation needs to assume that the internal interface between the 2 layers is homogeneous outside the defect and that the defect is a finite part of this interface with another homogeneous behavior. By a homogeneous behavior, we mean that the physical conditions to be satisfied on both sides of a surface between 2 media (the healthy interface or the finite defect) do not depend on the coordinate(s) along it. In practice, it will be assumed that the internal interface fulfills a perfect adhesion between the 2 solids, whereas the finite defect yields a delamination or a partial bonding with constant characteristics of the glue.

The principle and the validity of the Kirchhoff approximation are first presented in Section II-A, independently of the method employed to calculate the different acoustic fields. Then some reminders are given in Section II-B on practical tools (decomposition of a beam into plane waves which leads to Fourier integrals, propagation of plane waves in anisotropic media, boundary conditions for plane waves). Finally, these tools are used in Section II-C to implement the Kirchhoff approximation using Fourier integrals.

### *A. Principle and Validity of the Kirchhoff Approximation*

*1) The Principle of the Method:* The Kirchhoff approximation, superscript $(k)$, may be explained on the basis of a "re-emission principle" for the (unknown) exact solution of the problem, superscript $(e)$.

*a) The passive re-emission principle:* Let us denote by $\mathbf{u}^{\alpha}$ the displacement field in the medium $\alpha$ ($\alpha = 0,1,2,3$), see Fig. 1. If the exact solution $\mathbf{u}^{\alpha(e)}$ of the problem of the interaction with the bilayered structure (including its finite defect) were known, this exact solution could be split into different terms in each medium. As an example, in the external fluid 0, we distinguish the incident field $\mathbf{u}_{\text{inc}}^{0}$ produced by the emitter and the global reflected field $\mathbf{u}_{\text{ref}}^{0(e)}$. In the fluid 3, only one transmitted field $\mathbf{u}_{\text{tr}}^{3(e)}$ exists. In each solid layer of the structure, the total field may be separated into 2 parts: one propagating toward the increasing coordinate $x_3$ (the "$a$" subscript) and the other propagating toward the decreasing $x_3$ (the "$b$" index): $\mathbf{u}_{a}^{\alpha(e)}$ and $\mathbf{u}_{b}^{\alpha(e)}$, $\alpha = 1,2$.

Now, let us assume that the values of the field $\mathbf{u}_{b}^{1(e)}$ all along the interface II are known, i.e., for $x_3 = h_1$ and for any value of the coordinate $x_1$. We may consider the half-space $x_3 \leq h_1$ as made up by the medium of the solid 1, and then calculate in this infinite region the solution of the propagation equations that takes these known values of $\mathbf{u}_{b}^{1(e)}$ on the plane $x_3 = h_1$ and that satisfies the radiation condition toward the negative values of $x_3$. Because this solution is unique, it coincides with the field $\mathbf{u}_{b}^{1(e)}(x_1, x_3)$ in the whole layer 1.

Once this field $\mathbf{u}_{b}^{1(e)}$ has been determined in the layer 1, it may be considered as an "incident" field on the upper interface I, together with the true incident field $\mathbf{u}_{\text{inc}}^{0}$. One then obtains a "reflected" field in the solid 1, which coincides with the field $\mathbf{u}_{a}^{1(e)}(x_1, x_3)$, and a "transmitted" field in the fluid 0, that is nothing but the true reflected field $\mathbf{u}_{\text{ref}}^{0(e)}$.

The same argument may be followed, assuming that the exact values of the field $\mathbf{u}_{a}^{2(e)}$ on the interface II are known, then calculating the field $\mathbf{u}_{a}^{2(e)}(x_1, x_3)$ in the whole layer 2 and again the interaction of this field with the third interface III, thus getting the fields $\mathbf{u}_{b}^{2(e)}$ and $\mathbf{u}_{\text{tr}}^{3(e)}$.

Actually, the exact values of the fields $\mathbf{u}_{b}^{1(e)}$ and $\mathbf{u}_{a}^{2(e)}$ are not known on the (only piecewise homogeneous) interface II. But if some approximate values $\mathbf{u}^{(\text{app})}(x_1, x_3 = h_1)$ may be obtained for these fields on this interface, then, following the procedure just described above, one may expect to determine approximate values $\mathbf{u}^{(\text{app})}(x_1, x_3)$ of the various fields and especially of the approximate value $\mathbf{u}_{\text{ref}}^{(\text{app})}$ of the exact reflected field.

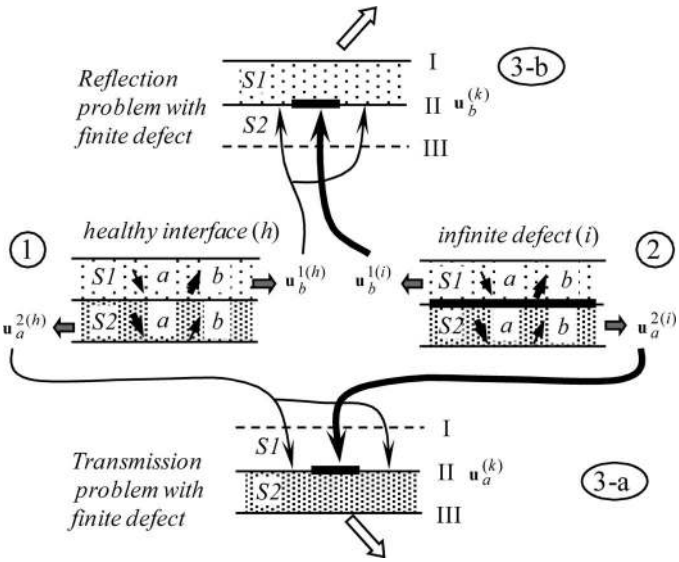


Fig. 2. Principle of the Kirchhoff approximation: passive re-emission principle.

*b) The Kirchhoff approximation:* The Kirchhoff approximation follows the process just described at the end of Section II-A-1-a and summed up in Fig. 2. The calculus of the approximate values of the fields on the interface II needs to solve 2 preliminary problems (the solution of which are given in Section II-C-1). As it has been said at the beginning of Section II, these problems will be introduced under the hypotheses of homogeneous behaviors of the interface II, on its healthy part on the one hand, and on its defective finite part on the other hand.

The first preliminary problem concerns the interaction between the incident field $\mathbf{u}_{\text{inc}}^{0}$ and the bi-layered structure with its internal interface II supposed to be healthy (without any defect, see part 1 of Fig. 2). The solution of this problem is available for any incident plane wave, hence for any incident field that may be expressed by a summation of plane waves. The solution of this first preliminary problem will be denoted $\mathbf{u}^{(h)}$.

The second preliminary problem is identical to the previous one, but with the homogeneous boundary conditions of the healthy interface replaced here by the homogeneous conditions of the defect, all along the interface; see part 2 of Fig. 2. Thus, we may speak of an "infinite defect" and the solution of this problem will be denoted $\mathbf{u}^{(i)}$.

The Kirchhoff approximation $\mathbf{u}^{(k)}$ of the exact solution $\mathbf{u}^{(e)}$ consists in choosing the approximate values for the fields on the interface II in the following way (Fig. 2): the field $\mathbf{u}_{b}^{1(k)}$ will be taken equal to the solution $\mathbf{u}_{b}^{1(i)}$ on the defect and to the solution $\mathbf{u}_{b}^{1(h)}$ outside for the reflection

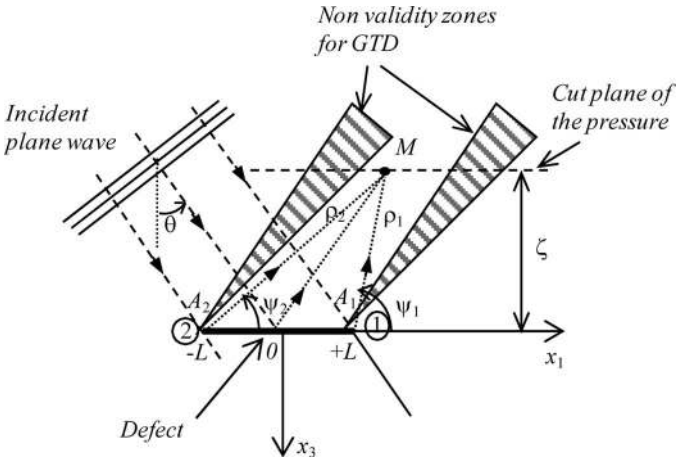


Fig. 3. Interaction of a plane wave (incident angle $\theta$) with a plane defect (length $2L$). GTD = Geometrical Theory of Diffraction.

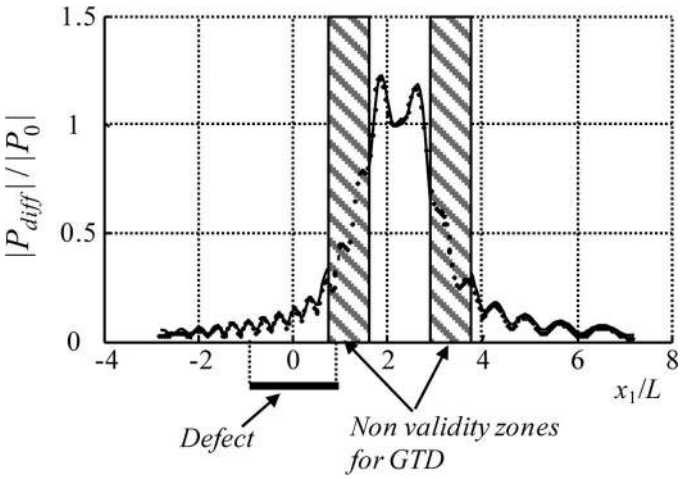


Fig. 4. Field diffracted by a zero pressure defect (length $2L$) in an infinite medium as a function of $x_1/L$ (see Fig. 3 for the geometry and the notations). $\theta = 20°$, $k_0L = 60$, $\zeta/L = 6$. Solid line: Geometrical Theory of Diffraction (GTD); dotted line: the Kirchhoff approximation; hatched regions: nonvalidity zones for GTD.

problem (see part 3-a of Fig. 2). Similarly, the field $\mathbf{u}_a^{2(k)}$ will be taken equal to the solution $\mathbf{u}_a^{2(i)}$ on the defect and to $\mathbf{u}_a^{2(h)}$ outside for the transmission problem (see part 3-b of Fig. 2). Then, the calculus of the fields re-emitted in the relevant half-spaces (following the procedure described in Section II-A-1-a) is performed. This re-emission is then followed by the interaction with the external interfaces I and III, and, therefore, the approximate solution $\mathbf{u}^{(k)}$ of the exact field $\mathbf{u}^{(e)}$ is obtained.

*2) Discussion of the Validity Domain of the Kirchhoff Approximation:* The validity of the Kirchhoff approximation may be appreciated by some physical considerations. Strictly speaking, the incident waves on each edge of the defect produce some diffraction effects that modify the field $\mathbf{u}^{(h)}$ on the healthy side of the interface and the field $\mathbf{u}^{(i)}$ on the defect side. Thus, the Kirchhoff approximation consists of ignoring these diffraction effects. It should be noted that neglecting these diffraction effects of the incident waves is clearly reasonable if the wavelength is small compared with the length $2L$ of the defect and if the incident direction is not too far from the normal direction to the plane of the defect.

*a) Comparison with the Theory of Diffraction:* A comparison between the Kirchhoff approximation and the Geometrical Theory of Diffraction (GTD) of Keller [17], [18], which is also a high-frequency method, may be carried out: because the GTD method takes into account the diffraction of the incident waves on each edge of the defect, it is interesting to be able to estimate the errors produced by the Kirchhoff approximation when neglecting these diffraction effects. With this in mind, we consider an infinite fluid medium (Fig. 3) with a finite straight line of length $2L$ (the defect) on which the acoustic pressure is assumed to be equal to zero. Fig. 4 shows the profiles of acoustic pressure modulus calculated both by the GTD method (the solid line) and by the Kirchhoff approximation (the dotted line), for an incident monochromatic plane wave (angular frequency denoted $\omega$) propagating in a fluid medium (speed of sound denoted $V^0$).

We recall that, in the GTD approach, the field is obtained by considering 3 rays: the specular reflected ray on the defect surface and the 2 rays resulting from the diffraction by the 2 edges of the defect (Fig. 3). The expressions for these diffraction fields may be found in [18]. For example, the diffraction pressure field (divided by the incident pressure) $\tilde{p}_{s_j}(M)$ coming from the edge $j$ ($j = 1,2$) at point $M$ (Fig. 3), can be written in the following form [omitting the term $\exp(i\omega t)$] [18].

On the other hand, the Kirchhoff approximation leads to the prediction of diffraction phenomena that appear in the solutions of the re-emission problems in solids 1 and 2, due to the discontinuity of the given (approximate) boundary values on the plane II.

$$\tilde{p}_{s_j}(M) = \frac{\varepsilon}{\sqrt{2\pi K_0 \tilde{\rho}_j}} \frac{\sqrt{(1+\varepsilon\cos\psi_j)(1-\varepsilon\sin\theta)}}{\sin\theta - \cos\psi_j} \times \exp\left\{-i\left[K_0(\tilde{\rho}_j + \varepsilon\sin\theta) + \frac{\pi}{4}\right]\right\} \times \left\{1 + \frac{i}{2K_0\tilde{\rho}_j}\frac{1-\cos\psi_j\sin\theta}{(\sin\theta-\cos\psi_j)^2} + O\left[(K_0\tilde{\rho}_j)^{-2}\right]\right\}, \quad (1)$$

where $\theta$, $\psi_j$, and $O[X^N]$ are, respectively, the incident angle, the angle between the $(Ox_1)$-axis and $\overrightarrow{A_jM}$, and a term of the $N$th-order in $X$, and where $k_0$, $K_0$, $\tilde{\rho}_j$, and $\varepsilon$ are given, respectively, by $k_0 = \omega/V^0$, $K_0 = k_0L$, $\tilde{\rho}_j = \rho_j/L$, $\varepsilon = 1$ for $j = 1$ and $\varepsilon = -1$ for $j = 2$.

It can be seen from (1) that the GTD solution $\tilde{p}_{s_j}(M)$ is not defined when $\theta = \psi_j + \pi/2$ (the solution is singular on the 2 lines corresponding to the reflected rays at the edges of the defect), which leads to nonvalidity zones for the GTD (Figs. 3 and 4).

When the plane defect consists of a slit with zero pressure, the geometrical reflected field can be easily calculated on the reflected rays on the slit. This field (divided by the incident pressure) at point $M(x_1,x_3)$ is given by

$$\tilde{p}_{\text{ref}}(M) = -\exp\left(-ik_0 x_1 \sin\theta + ik_0 x_3 \cos\theta\right). \quad (2)$$

The total pressure is the summation of the geometrical reflected field $\tilde{p}_{\text{ref}}(M)$ and of the field which is scattered by each edge 1 and 2, i.e., $\tilde{p}_{s_1}(M)$ and $\tilde{p}_{s_2}(M)$ (Fig. 3):

$$\tilde{p}_{\text{GTD}}(M) = \tilde{p}_{\text{ref}}(M) + \tilde{p}_{s_1}(M) + \tilde{p}_{s_2}(M). \quad (3)$$

For example, for an incident angle $\theta$ equal to 20° and an adimensional frequency $K_0 = k_0 L = 60$ (Fig. 4), the comparison between the 2 methods is fairly good in the main part of the reflected field, but also for the diffraction patterns on the left and right parts of the pressure profiles.

This simple case, without any mode conversion, permits to evaluate the error made on the solution, which results from the fact that a part of the diffraction effects are omitted; these diffraction effects are taken into account by the GTD but are not when using Kirchhoff's approximation. Similar cases can be found in the literature for defects in isotropic or anisotropic solids (see [19] and references contained therein).

*b) Comparison with results from a boundary finite element method:* The validity of the Kirchhoff approximation may be evaluated by comparison with results obtained through a boundary finite element method. In [20] and [21], a Fourier transform/boundary element hybrid method has been introduced for the simplified case where the 2 layers are made of the same isotropic material. The comparison shows that for all the geometrical configurations, the results fit each other in the main part of the reflected field, whereas some discrepancy may appear in the side parts where diffraction effects dominate. As expected, this discrepancy diminishes when the length of the defect is increased or at higher frequencies.

### *B. The Method of Plane Wave Decomposition*

Before using the Kirchhoff approximation, some practical tools have to be described to obtain the different acoustic fields corresponding to the 2 preliminary problems mentioned in Section II-A-1-b.

1. The incident-bounded beam has to be decomposed into monochromatic plane waves (via Fourier transforms) and the displacement and stress fields have to be expressed in a coordinate system linked to the layered structure (see Section II-B-1-a). Because the method chosen here to calculate Fourier transforms is the fast Fourier transform algorithm, Section II-B-1 ends with some considerations about the use of this algorithm (see Section II-B-1-b).
2. The displacement fields in an anisotropic bilayered structure immersed in a fluid have to be obtained, and this involves writing a) the displacement and stress fields in an anisotropic medium with appropriate radiation conditions (see Section II-B-2) and b) the boundary conditions (including bonding conditions) at the interface separating 2 anisotropic media (see Section II-B-3).

To be more concise, we made the choice in this paper to treat only the reflection problem in fluid 0, but similar expressions can be easily obtained for the transmission problem in fluid 3. In addition, it should be noted that this case is the classic case of interest in NDT when the reflected field is the only accessible field that can be measured.

*1) The Incident Bounded Beam in Fluid 0: a) Principle of the decomposition into plane waves and change of basis:* The principle of the decomposition of a beam into monochromatic waves (or angular spectrum decomposition) is a well-known principle that can be applied to a scalar or a vector field [22]–[36], based on the linearity of the wave equations considered. Here, the incident displacement field $\mathbf{u}^0_{\text{inc}}$ can be built, at any point $M(X_1^E, X_3^E)$, omitting the $\exp(i\omega t)$ factor, as a superposition of all the plane acoustic fields with parameter $K_1^E$. Its expression can be written as

$$\mathbf{u}^0_{\text{inc}}(X_1^E, X_3^E) = \int_{-\infty}^{+\infty} \left\{ \hat{A}^E(K_1^E) \frac{\mathbf{k}^0(K_1^E)}{k^0} \exp\left[-i(K_1^E X_1^E + K_3^{0E} X_3^E)\right] \mathrm{d}K_1^E \right\}, \quad (4)$$

where $\hat{A}^E(K_1^E)$ is the amplitude of each plane wave and where $(K_1^E, 0, K_3^{0E})$ are the components of the wave vector $\mathbf{k}^0$ of the fluid 0 (angular frequency $\omega$) in the coordinate system $R^E = (O^E, X_1^E, X_2^E, X_3^E)$ linked to the emitting transducer (Fig. 1). These components satisfy the dispersion relation

$$(K_1^E)^2 + (K_3^{0E})^2 = \|\mathbf{k}^0\|^2 = (k^0)^2 = (\omega/V^0)^2, \quad (5)$$

where $V^0$ is the speed of the waves propagating in the fluid 0.

The particle displacement $u_{3_{\text{inc}}}^{0E}(X_1^E, 0)$ in the fluid, normal to the front face of the emitting transducer, is assumed to be known and can be derived from experimental results or analytical expression.

Using (4), the displacement $u_{3_{\text{inc}}}^{0E}(X_1^E, 0)$ can be written as

$$u_{3_{\text{inc}}}^{0E}(X_1^E, 0) = \int_{-\infty}^{+\infty} \left\{ \hat{A}^E(K_1^E) \frac{K_3^{0E}}{k^0} \exp\left(-iK_1^E X_1^E\right) \mathrm{d}K_1^E \right\}, \quad (6)$$

which permits, by means of an inverse Fourier transform, obtaining the angular spectrum $U_{3_{\text{inc}}}^{0E}$, and thus the amplitudes $\hat{A}^{E}\left(K_1^E\right)$:

$$U_{3_{\text{inc}}}^{0E}\left(K_1^E\right) = \hat{A}^{E}\left(K_1^E\right)\frac{K_3^{0E}}{k^0} = \frac{1}{2\pi}\int_{-\infty}^{+\infty} u_{3_{\text{inc}}}^{0E}\left(X_1^E,0\right)\exp\left(iK_1^E X_1^E\right)\mathrm{d}X_1^E. \tag{7}$$

To study the interaction of each monochromatic plane wave with the 2-layered structure, a change of coordinate system is necessary, the new one $R = \left(O, x_1, x_2, x_3\right)$ being linked to the structure (Fig. 1). The translation from the origin $O^E$ to the new one $O$ results in a change of phase $\exp\left(-i\mathbf{k}^0 \cdot \overrightarrow{O^E O}\right) = \exp\left(-iK_3^{0E}Z_0\right)$, and the rotation angle $\theta$ around the $x_2$-axis (corresponding to the incident angle of the acoustic beam) results in a Jacobian $J\left(k_1\right)$ such that

$$\mathrm{d}K_1^E = \left(\cos\theta + \frac{k_1}{k_3^0}\sin\theta\right)\mathrm{d}k_1 = J\left(k_1\right)\mathrm{d}k_1, \tag{8}$$

where $k_1$ and $k_3^0$ are the components of the wave number $\mathbf{k}^0$ on the $x_1$- and $x_3$-axes ($K_1^E$ and $K_3^{0E}$ are functions of $k_1$).

The amplitude $\hat{A}\left(k_1\right)$ of each incident plane wave, when referenced at the plane $x_3 = 0$ (interface I) can thus be expressed as a function of its amplitude $\hat{A}^{E}\left(K_1^E\right)$, and when referenced at the plane $X_3^E = 0$, by

$$\hat{A}\left(k_1\right) = \hat{A}^{E}\left(K_1^E\right)\exp\left(-iK_3^{0E}Z_0\right)J\left(k_1\right), \tag{9}$$

which leads to the following expression of the incident particle displacement in the fluid 0, in the coordinate system $R$:

$$\mathbf{u}_{\text{inc}}^{0}\left(x_1, x_3\right) = \int_{-\infty}^{+\infty}\left\{\hat{A}\left(k_1\right)\frac{\mathbf{k}^0\left(k_1\right)}{k^0}\exp\left[-i\left(k_1 x_1 + k_3^0 x_3\right)\right]\mathrm{d}k_1\right\}, \tag{10}$$

where $\mathbf{P}_{\text{inc}}^{0} = \mathbf{k}^0\left(k_1\right)/k^0$ is the polarization vector of the incident wave in fluid 0.

*b) Use of the fast Fourier transform algorithm:* The method used to calculate the Fourier transforms and inverse Fourier transforms is the fast Fourier transform (FFT). This algorithm imposes a constant step sampling. However, due to the rotation angle $\theta$ around the $x_2$-axis (corresponding to the incident angle of the acoustic beam) between the plane linked to the emitting transducer and the plane linked to the interfaces of the layered structure, a constant step sampling along $X_1^E$-axis (and thus for $K_1^E$) leads to a nonconstant step sampling along the $x_1$-axis (and thus for $k_1$), as it can be seen in the expression of the Jacobian $J\left(k_1\right)$ in (8).

Two methods can be used to obtain the amplitudes $\hat{A}\left(k_1\right)$ [given by (9)] of each incident plane wave (referenced at the plane $x_3 = 0$) for a constant step sampling for $k_1$. The first one consists in calculating the angular spectrum $U_{3_{\text{inc}}}^{0E}\left(K_1^E\right)$ [given by (7)], then the Jacobian $J\left(k_1\right)$, and finally the amplitudes $\hat{A}\left(k_1\right)$, with a constant step sampling for $K_1^E$ (which gives a nonconstant step sampling for $k_1$). An interpolation of the amplitudes $\hat{A}\left(k_1\right)$ is then provided to obtain new amplitudes $\hat{A}\left(k'_1\right)$, corresponding to a constant step sampling for $k'_1$.

The second method consists in interpolating the angular spectrum $U_{3_{\text{inc}}}^{0E}\left(K_1^E\right)$ to obtain new values $U_{3_{\text{inc}}}^{0E}\left(K'_1{}^E\right)$ corresponding to a nonconstant step sampling in $K'_1{}^E$, but corresponding to a constant step sampling in $k_1$. The Jacobian $J\left(k_1\right)$ and the amplitudes $\hat{A}\left(k_1\right)$ are then calculated with this constant step sampling in $k_1$. It has been shown [50] that this second method gives more accurate results than the first one.

In other words,

1. $U_{3_{\text{inc}}}^{0E}\left(K_1^E\right)$ is calculated from (9) and using a constant step sampling in $K_1^E$,
2. $U_{3_{\text{inc}}}^{0E}\left(K_1^E\right)$ is interpolated to obtain $U_{3_{\text{inc}}}^{0E}\left(K'_1{}^E\right)$, using the nonconstant step sampling in $K'_1{}^E$ which gives a constant step sampling in $k_1$.

*c) Subsequent use of the decomposition method:* The method of decomposition of a beam into plane waves that has just been described in Section II-B-1-a is also used to calculate the field re-emitted by the finite-sized defect, following the passive re-emission principle described in Section II-A-1-a. This calculation requires that the re-emission data on the interface II admit a Fourier integral, which is ensured by introducing a scattering problem in Section II-C for which the data are zero outside of the defect.

*2) Plane Waves in Anisotropic Media:* Generally speaking, the interaction between an oblique incident monochromatic plane wave propagating in the plane $(Ox_1x_3)$ and an anisotropic layered structure generates 6 plane waves [numbered by $(\eta)$] in each layer, with different velocities. The propagation equations in each layer use the same form as the one developed by Rokhlin *et al.* [37], [38] and completed by Ribeiro *et al.* [39] with the help of the inhomogeneous waveform [40], [41].

It is useful to introduce the slowness vector ${}^{(\eta)}\mathbf{m}$ of the wave $(\eta)$, defined by [42], [43]

$${}^{(\eta)}\mathbf{m} = {}^{(\eta)}\mathbf{n}/{}^{(\eta)}V = {}^{(\eta)}\mathbf{k}/\omega, \tag{11}$$

where ${}^{(\eta)}\mathbf{n}$, ${}^{(\eta)}\mathbf{k}$ and ${}^{(\eta)}V$ are respectively the propagation direction vector, the wave vector and the velocity of the

wave ($\eta$) in the considered layer. It should be noted that, due to the boundary conditions at each interface (I, II, or III) which lead to Snell-Descartes' laws, the projections $m_1$ and $m_2$ of the slowness vector of all the waves on $x_1$ and $x_2$-axis are the same (with here $m_2 = 0$).

In each anisotropic layer, the displacement vector ${}^{(\eta)}\mathbf{U}$ of each plane wave ($\eta$) has the following form

$$\begin{aligned} {}^{(\eta)}\mathbf{U}(x_1, x_3; t) &= {}^{(\eta)}a\,{}^{(\eta)}\mathbf{P} \exp\Big[-i\Big(k_1 x_1 + {}^{(\eta)}k_3 x_3 - \omega t\Big)\Big] \\ &= {}^{(\eta)}a\,{}^{(\eta)}\mathbf{P} \exp\Big[-i\omega\Big(m_1 x_1 + {}^{(\eta)}m_3 x_3 - t\Big)\Big], \end{aligned} \tag{12}$$

where ${}^{(\eta)}a$ and ${}^{(\eta)}\mathbf{P}$ are, respectively, the amplitude and the polarization vector of the wave ($\eta$), $m_1$, and ${}^{(\eta)}m_3$ are the components on axes $x_1$ and $x_3$, respectively, of the slowness vector ${}^{(\eta)}\mathbf{m}$.

Using Hooke law in anisotropic solid media (and summation convention on repeated indexes), the stresses can be expressed as functions of displacements by

$${}^{(\eta)}T_{ij} = c_{ijk\ell} \frac{\partial\, {}^{(\eta)}U_\ell}{\partial x_k}, \tag{13}$$

where the $c_{ijkl}$ are the elastic constants of the layer. The stress vector ${}^{(\eta)}\mathbf{T}$ (associated with the normal $\mathbf{e}_{x_3}$ to the interfaces) of each plane wave ($\eta$) has the following form

$${}^{(\eta)}\mathbf{T} = {}^{(\eta)}T_{i3}\mathbf{e}_{x_i}. \tag{14}$$

Following the principle of the Kirchhoff approximation explained in Section II-A-1, it is necessary to identify in each layer the waves that propagate (or decrease) in the direction $x_3 > 0$ (denoted "$a$") and those that propagate (or decrease) in the direction $x_3 < 0$ (denoted "$b$"). For propagative waves, this identification must be done by using an energetic criterion [44]–[46], based on the sign of the normal power flux given by Synge [47]:

$${}^{(\eta)}F_3 = -\frac{1}{4} i\omega\Big(-T_{3j}U_j^* + T_{3j}^* U_j\Big), \tag{15}$$

where $X^*$ is the complex conjugate of $X$. For inhomogeneous waves, a decreasing condition must be applied, using the sign of the imaginary part ${}^{(\eta)}m''_3$ of the 3rd component ${}^{(\eta)}m_3$ of the slowness vector of the wave ($\eta$). Subsequently, for convenience, the indexes $\eta = 1,2,3$ will refer to "$b$" waves that propagate (or decrease) in the direction $x_3 < 0$, and $\eta = 4,5,6$ will refer to "$a$" waves that propagate (or decrease) in the direction $x_3 > 0$. The energetic and radiation criteria can thus be summarized as follows:

$$\text{field } b,\ \eta = 1,2,3 \begin{cases} {}^{(\eta)}F_3 < 0, & \text{propagative waves,} \\ {}^{(\eta)}m''_3 > 0, & \text{inhomogeneous waves,} \end{cases} \tag{16a}$$

$$\text{field } a,\ \eta = 4,5,6 \begin{cases} {}^{(\eta)}F_3 > 0, & \text{propagative waves,} \\ {}^{(\eta)}m''_3 < 0, & \text{inhomogeneous waves.} \end{cases} \tag{16b}$$

*3) Plane Waves Transmitted Through Interfaces (Boundary Conditions, Including Bonding Conditions, at Interface II):* In case of a perfect (rigid) bonding between solid media 1 and 2 at the interface II, the boundary conditions consist in the continuity of the displacement and stress vectors (associated with the normal $\mathbf{e}_{x_3}$ to the interfaces), i.e.,

$$\mathbf{U}^1(x_1, x_3 = h_1; t) = \mathbf{U}^2(x_1, x_3 = h_1; t), \tag{17a}$$

$$\text{and } \mathbf{T}^1(x_1, x_3 = h_1; t) = \mathbf{T}^2(x_1, x_3 = h_1; t), \quad \forall x_1, x_3 = h_1, \quad \forall t. \tag{17b}$$

Conditions (17) are those involved in the preliminary problem solved for a healthy interface II (see Section II-A-1-b and Section III-C-1)

In case of a total delamination at interface II, the boundary conditions consist of setting the stress vectors to zero, i.e.,

$$\mathbf{T}^1(x_1, x_3 = h_1; t) = \mathbf{0}, \quad x_3 = h_1, \forall t, \tag{18a}$$

$$\text{and } \mathbf{T}^2(x_1, x_3 = h_1; t) = \mathbf{0}, \quad x_3 = h_1, \quad \forall t, \tag{18b}$$

for all the values of $x_1$ corresponding to points on the defect.

In case of intermediate (elastic) bonding between solid media 1 and 2 at the interface II (which is the case of the defects considered here), the boundary conditions chosen here depend on those introduced by Pilarski *et al.* [7] and widely used from that time. In a bidimensional case, these bonding conditions consist in schematizing the bonding by a uniform distribution of springs without mass working under traction-compression and shear deformation [48], [49]. Using the stress vector associated with the normal $\mathbf{e}_{x_3}$ to the interfaces and defined by (14), a linear relation between the stress vector and a shift of displacements $\Delta\mathbf{U}$ can thus be written such that

$$\mathbf{T}^1(x_1, x_3 = h_1; t) = \mathbf{T}^2(x_1, x_3 = h_1; t), \quad x_3 = h_1, \quad \forall t, \tag{19a}$$

$$\mathbf{U}^1(x_1, x_3 = h_1; t) \neq \mathbf{U}^2(x_1, x_3 = h_1; t), \quad x_3 = h_1, \quad \forall t, \tag{19b}$$

$$\mathbf{T}^1(x_1, x_3 = h_1; t) = \mathbf{K}\,\Delta\mathbf{U}(x_1, x_3 = h_1; t), \quad x_3 = h_1, \quad \forall t, \tag{19c}$$

for all the values of $x_1$ corresponding to points on the defect, where

$$\Delta\mathbf{U} = \mathbf{U}^2 - \mathbf{U}^1 \tag{20}$$

and $\mathbf{K}$ is a $(3 \times 3)$ matrix of stiffness coefficients. In practice, the coupling between traction/compression and shear effects can be ignored, so that the matrix $\mathbf{K}$ can be considered as a diagonal matrix. It should be noted that the positive signs of the coefficients of the matrix $\mathbf{K}$ are straightforwardly associated with the direction of the nor-

mal $\mathbf{e}_{x_3}$, which points out from medium 1 toward medium 2.

Conditions (19) are assumed to be those on the finite-sized defect on interface II. To solve the preliminary problem for an infinite defect on interface II (see Section II-A-1 and Section II-C-1), these conditions (19) are extended all along interface II.

Once the Kirchhoff approximation principle is explained and the practical tools for calculating the acoustic fields using plane waves are given, the following Section II-C aims at presenting the implementation of the Kirchhoff approximation method (such as it has been described in Section II-A) using Fourier integrals: the 2 preliminary problems have to be solved (Section II-C-1) and the scattering problem is then introduced (Section II-C-2).

### *C. Implementation of the Kirchhoff Approximation Using Plane Wave Decomposition*

To be more concise, we made the choice in this paper to treat only the reflection problem in fluid 0, but similar expressions can be easily obtained for the transmission problem in fluid 3. The parametric study in Section III deals only with this reflected field.

As explained in Section II-A-1-b, the Kirchhoff approximation needs to solve 2 preliminary problems: the first one concerns the interaction between the incident field $\mathbf{u}_{\text{inc}}^{0}$ and the bilayered structure with its internal interface II supposed to be healthy (without any defect); the second preliminary problem is identical to the previous one, but with an "infinite defect" at interface II; this is the aim of Section II-C-1 to explicitly treat these preliminary problems, first for plane waves and second for bounded beams. Finally, as mentioned in Section II-B-1-c, a scattering problem has to be introduced (see Section II-C-2), to ensure that the re-emission data on the interface II would admit a Fourier integral.

#### *1) Solution of Preliminary Problems:*

*a) Solution of preliminary problems for plane waves:* These 2 preliminary problems must be first solved for each monochromatic plane wave constituting the incident-bounded beam, the amplitude of each plane wave being equal to $\hat{A}(k_1)$ [see (9), Section II-B-1-a]. For each problem, 14 scalar equations derived from the boundary conditions must be written, using notations defined in Section II-B-2, as follows.

1. Four equations coming from the continuity of the component on $x_3$-axis of the displacement vector $\mathbf{U}$ and from the continuity of the stress vector $\mathbf{T}$ at interface I (fluid 0/solid 1):

$$U_3^0(x_1, x_3 = 0; t) = U_3^1(x_1, x_3 = 0; t), \quad \forall x_1, x_3 = 0, \quad \forall t, \tag{21a}$$

$$\mathbf{T}^0(x_1, x_3 = 0; t) = \mathbf{T}^1(x_1, x_3 = 0; t), \quad \forall x_1, x_3 = 0, \quad \forall t. \tag{21b}$$

2. Four similar equations at interface III (solid 2/fluid 3)
3. Six equations derived from the boundary conditions (19) at interface II (solid 1/solid 2), whether this interface is healthy or consists of an infinite defect

Fourteen unknown amplitudes correspond to these 14 boundary conditions: the amplitude $a_{\text{ref}}^{0}$ of the wave reflected in fluid 0, the 12 amplitudes ${}^{(\eta)}a^{\alpha}$ of the waves propagating or decreasing in each layer $\alpha$, $\alpha = 1,2$ (6 per layer), and the amplitude $a_{tr}^{3}$ of the wave transmitted in fluid 3.

The 2 preliminary problems for plane waves can thus be solved: the problem (*) with a healthy interface II [(*) = $(h)$] or an infinite defect [(*) = $(i)$] on that interface. In particular, the solutions for plane waves $\mathbf{U}^{\boldsymbol{\alpha}(*)}$ of the problem (*) can be split, in each layer $\alpha$ ($\alpha = 1,2$), into the solutions $\mathbf{U}_a^{\alpha(*)}$ and $\mathbf{U}_b^{\alpha(*)}$ corresponding to the waves propagating or decreasing toward $x_3 > 0$ (or $x_3 < 0$), respectively:

$$\mathbf{U}^{\alpha(*)} = \mathbf{U}_a^{\alpha(*)} + \mathbf{U}_b^{\alpha(*)}, \quad \alpha = 1,2, \tag{22a}$$

where [omitting the $\exp(i\omega t)$ factor and using (13)]

$$\begin{aligned}\mathbf{U}_a^{\alpha(*)} &= \sum_{\eta=4}^{6} {}^{(\eta)}\mathbf{U}_a^{\alpha(*)} \\ &= \sum_{\eta=4}^{6} {}^{(\eta)}a^{\alpha(*)\,(\eta)}\mathbf{P}^{\alpha} \exp\left[-i\left(k_1 x_1 + {}^{(\eta)}k_3^{\alpha} x_3\right)\right], \\ &\qquad \alpha = 1,2,\end{aligned} \tag{22b}$$

and

$$\begin{aligned}\mathbf{U}_b^{\alpha(*)} &= \sum_{\eta=1}^{3} {}^{(\eta)}\mathbf{U}_b^{\alpha(*)} \\ &= \sum_{\eta=1}^{3} {}^{(\eta)}a^{\alpha(*)\,(\eta)}\mathbf{P}^{\alpha} \exp\left[-i\left(k_1 x_1 + {}^{(\eta)}k_3^{\alpha} x_3\right)\right], \\ &\qquad \alpha = 1,2,\end{aligned} \tag{22c}$$

using criteria (26) (see Section II-B-2).

It should be noted that the amplitudes ${}^{(\eta)}a^{\alpha(*)}$ are function of amplitude $\hat{A}(k_1)$ of each incident plane wave constituting the incident-bounded beam. Therefore, it could be convenient to write them in the form

$${}^{(\eta)}a^{\alpha(*)}(k_1) = \hat{A}(k_1)\,{}^{(\eta)}T^{\alpha(*)}, \tag{23}$$

where ${}^{(\eta)}T^{\alpha(*)}$ are amplitude ratios.

*b) Solution of preliminary problems for bounded beams:* Finally, the fields corresponding to the incident-bounded beam can be obtained by superposing the fields obtained

in Section II-C-1-a for plane waves, using the superposition principle as explained in Section II-B-1.

In particular, the field $\mathbf{u}^{\boldsymbol{\alpha}(*)}$ in layer $\alpha$ ($\alpha = 1,2$) of the problem (*) can be written such that

$$\mathbf{u}^{\alpha(*)} = \mathbf{u}_a^{\alpha(*)} + \mathbf{u}_b^{\alpha(*)}, \quad (*) = (h) \text{ or } (*) = (i), \tag{24a}$$

where

$$\mathbf{u}_a^{\alpha(*)}(x_1, x_3) = \sum_{\eta=4}^{6} \int_{-\infty}^{+\infty} \left\{ \hat{A}(k_1)\, {}^{(\eta)}T^{\alpha(*)}(k_1)\, {}^{(\eta)}\mathbf{P}^{\alpha} \times \exp\left(-i\, {}^{(\eta)}k_3^{\alpha} x_3\right) \exp\left(-ik_1 x_1\right) \right\} \mathrm{d}k_1, \tag{24b}$$

and

$$\mathbf{u}_b^{\alpha(*)}(x_1, x_3) = \sum_{\eta=1}^{3} \int_{-\infty}^{+\infty} \left\{ \hat{A}(k_1)\, {}^{(\eta)}T^{\alpha(*)}(k_1)\, {}^{(\eta)}\mathbf{P}^{\alpha} \times \exp\left(-i\, {}^{(\eta)}k_3^{\alpha} x_3\right) \exp\left(-ik_1 x_1\right) \right\} \mathrm{d}k_1. \tag{24c}$$

Eqs. (24b) and (24c) will be used in Section II-C, when solving the scattering problem (27).

It is convenient to write here the expression of the reflected displacement field, for the problem with a healthy interface II [(*) = ($h$)] or an infinite defect on interface II [(*) = ($i$)]:

$$\mathbf{u}_{\mathrm{ref}}^{0(*)}(x_1, x_3) = \int_{-\infty}^{+\infty} \left\{ a_{\mathrm{ref}}^{0(*)}(k_1)\, \mathbf{P}_{\mathrm{ref}}^{0} \exp\left(+ik_3^0 x_3\right) \times \exp\left(-i\mathbf{k}_1 x_1\right) \mathrm{d}k_1 \right\}, \tag{25}$$

where $\mathbf{P}_{\mathrm{ref}}^{0}$ is the polarization vector of the reflected wave in fluid 0. Eq. (25) will be used subsequently in Section II-C-3 to calculate the pressure $P_{\mathrm{ref}}^{0(*)}$ in fluid 0 [see (40)].

*2) The Associated Scattering Problem:* Once the approximate values $\mathbf{u}^{(k)}$ have been obtained on the interface II, by considering the solutions $\mathbf{u}^{(h)}$, and $\mathbf{u}^{(i)}$ of the 2 preliminary problems mentioned in Section II-A-1-b (the solution of which is given in Section II-C-1), we need to solve the radiation problems in the 2 (virtual) half-spaces $x_3 \leq h_1$ and $x_3 \geq h_1$. To calculate the solutions of these radiation problems, a plane wave decomposition of the field may be introduced by the way of a spatial Fourier transform along the line $x_3 = h_1$. This Fourier transform will be easily defined if an associated scattering problem is introduced, considering the field generated by the defect as a perturbation of the field of the healthy structure. Thus, the approximate global solution may be sought in the form of a sum:

$$\mathbf{u}^{(k)} = \mathbf{u}^{(h)} + \mathbf{u}^{(s)}, \tag{26}$$

where $\mathbf{u}^{(s)}$ is a scattering term that must be calculated by the above-described procedure. For this scattering problem, the (approximate) values of the fields on the interface II are:

$$\begin{cases} \mathbf{u}_b^{1(s)}(x_1, x_3 = h_1) = \mathbf{0} & \text{outside the defect,} \quad (27a) \\ \mathbf{u}_b^{1(s)}(x_1, x_3 = h_1) = \mathbf{u}_b^{1(i)} - \mathbf{u}_b^{1(h)} & \text{on the defect,} \quad (27b) \end{cases}$$

which permits us to obtain $\mathbf{u}_b^{1(s)}(x_1, x_3)$ in layer 1 (see Section II-A-1-a, the passive re-emission principle). Similar expressions can also be written for the approximate field $\mathbf{u}_a^{2(s)}$.

Once the corresponding scattered field is calculated in the half space $x_3 \leq h_1$, by plane wave decomposition, one may consider its interaction with the interface I, getting the 2 "reflected" and "transmitted" scattered fields $\mathbf{u}_a^{1(s)}$ and $\mathbf{u}_{\mathrm{ref}}^{0(s)}$. Note that in the scattering problem, the incident field $\mathbf{u}_{\mathrm{inc}}^{0}$ no longer enters into the interaction with the interface I.

Finally, the expected total approximate reflected field is obtained by the following expression:

$$\mathbf{u}_{\mathrm{ref}}^{0(k)} = \mathbf{u}_{\mathrm{ref}}^{0(h)} + \mathbf{u}_{\mathrm{ref}}^{0(s)}. \tag{28}$$

*a) The scattering data on the interface II:* The solutions of the preliminary problems ($h$) and ($i$) have been obtained in Section II-C-1. It is now possible to apply the Kirchhoff approximation method (see Section II-A-1) to obtain the approximate solution $\mathbf{u}^{(k)}$.

It should be noted that, for the scattering problem (27), the fields $\mathbf{u}_b^{1(s)}(x_1, x_3 = h_1)$ and $\mathbf{u}_a^{2(s)}(x_1, x_3 = h_1)$ are perfectly known on the interface II, and that they constitute re-emission data for the reflection problem and the transmission problem, respectively.

Substituting (24c) for $x_3 = h_1$ in the scattering problem leads to expressions for the field $\mathbf{u}_b^{1(s)}(x_1, x_3 = h_1)$ on interface II (with the aim of determining the reflected field in fluid 0):

$$\mathbf{u}_b^{1(s)}(x_1, x_3 = h_1) = \mathbf{0}, \quad \text{outside the defect,} \tag{29a}$$

$$\mathbf{u}_b^{1(s)}(x_1, x_3 = h_1) = \sum_{\eta=1}^{3} \int_{-\infty}^{+\infty} \left\{ \hat{A}(k_1) \left[ {}^{(\eta)}T^{1(i)}(k_1) - {}^{(\eta)}T^{1(h)}(k_1) \right] \times {}^{(\eta)}\mathbf{P}^{1} \exp\left(-i\, {}^{(\eta)}k_3^{1} h_1\right) \exp\left(-ik_1 x_1\right) \mathrm{d}k_1 \right\}, \quad \text{on the defect,} \tag{29b}$$

which involve the difference of the amplitude ratios ${}^{(\eta)}T^{1(i)}(k_1)$ for the infinite defect problem and the amplitude ratios ${}^{(\eta)}T^{1(h)}(k_1)$ for the healthy interface II. Simi-

larly, the field $\mathbf{u}_a^{2(s)}(x_1, x_3 = h_1)$ can be obtained, with the view of solving the transmission problem.

*b) Resolution of the scattering problem:* Let us consider the problem of the re-emission toward $x_3 < 0$, to obtain the reflected scattered field $\mathbf{u}_{\text{ref}}^{0(s)}$ in fluid 0 and thus, using (27), the Kirchhoff approximation $\mathbf{u}_{\text{ref}}^{0(k)}$ of the exact solution.

With the radiation condition toward $x_3 < 0$, the field $\mathbf{u}_b^{1(s)}(x_1, x_3)$ is expressed in solid 1 in the form

$$\mathbf{u}_b^{1(s)}(x_1, x_3) = \sum_{\eta=1}^{3} \int_{-\infty}^{+\infty} \left\{ {}^{(\eta)}\hat{A}^{1(s)}(k_1)\, {}^{(\eta)}\mathbf{P}^1 \times \exp\left(-i\, {}^{(\eta)}k_3^1 x_3\right) \exp\left(-ik_1 x_1\right) \mathrm{d}k_1 \right\}, \tag{30}$$

where the amplitudes ${}^{(\eta)}\hat{A}^{1(s)}(k_1)$ are going to be determined from re-emission data (29), using exactly the same method as that explained in Section II-B-1 for the incident beam.

As $\mathbf{u}_b^{1(s)}(x_1, x_3 = h_1)$ is known on interface II, an inverse Fourier transform of (30) leads to the vector equation

$$\sum_{\eta=1}^{3} {}^{(\eta)}\hat{A}^{1(s)}(k_1)\, {}^{(\eta)}\mathbf{P}^1 \exp\left(-i\, {}^{(\eta)}k_3^1 h_1\right) = \frac{1}{2\pi} \int_{-\infty}^{+\infty} \mathbf{u}_b^{1(s)}(x_1, h_1) \exp\left(+ik_1 x_1\right) \mathrm{d}x_1, \tag{31}$$

which constitutes a linear system of 3 equations for the 3 unknown amplitudes ${}^{(\eta)}\hat{A}^{1(s)}(k_1)$, $\eta = 1,2,3$. It should be noted that the integrand of the right hand term of (31) is null outside the defect, because of (29a). Then, using (30), the whole field $\mathbf{u}_b^{1(s)}(x_1, x_3)$ is known in layer 1.

Similar expression can be obtained for the transmitted scattered field $\mathbf{u}_{\text{tr}}^{3(s)}$ in fluid 3.

*c) Interaction of the scattered field with interface I:* Now, following the re-emission principle (see Section II-A-1-a), the field $\mathbf{u}_b^{1(s)}(x_1, x_3)$ behaves like an "incident" field on the interface I at $x_3 = 0$, and the problem of the interaction of each plane wave constituting this "incident" beam with the interface I has to be solved.

Using (30), this "incident" beam $\mathbf{u}_b^{1(s)}(x_1, x_3 = 0)$ at $x_3 = 0$ can be written as (omitting $\exp(i\omega t)$ factor)

$$\mathbf{u}_b^{1(s)}(x_1, x_3 = 0) = \int_{-\infty}^{+\infty} \mathbf{U}_b^{1(s)}(k_1) \exp\left(-ik_1 x_1\right) \mathrm{d}k_1, \tag{32}$$

$$\text{where } \mathbf{U}_b^{1(s)}(k_1) = \sum_{\eta=1}^{3} {}^{(\eta)}\hat{A}^{1(s)}(k_1)\, {}^{(\eta)}\mathbf{P}^1 \tag{33}$$

is the angular spectrum (plane waves).

The interaction of these incident waves $\mathbf{U}_b^{1(s)}$ with interface I generates reflected waves $\mathbf{U}_a^{1(s)}$ (with 3 unknown amplitudes ${}^{(\eta)}a^{1(s)}$ ($\eta = 4,5,6$)) in medium 1 and a transmitted wave $\mathbf{U}^{0(s)}$ (with an unknown amplitude $a_{\text{ref}}^{0(s)}$) in fluid 0.

Thus, the whole field $\mathbf{U}^{1(s)}$ in solid 1 at $x_3 = 0$ is made up of the "incident" $b$-type waves $\mathbf{U}_b^{1(s)}$ propagating (or decreasing) toward $x_3 < 0$ and of the "reflected" $a$-type waves $\mathbf{U}_a^{1(s)}$ propagating (or decreasing) toward $x_3 > 0$:

$$\mathbf{U}^{1(s)}(k_1) = \mathbf{U}_a^{1(s)}(k_1) + \mathbf{U}_b^{1(s)}(k_1), \tag{34}$$

$$\text{where } \mathbf{U}_a^{1(s)}(k_1) = \sum_{\eta=4}^{6} {}^{(\eta)}a^{1(s)}(k_1)\, {}^{(\eta)}\mathbf{P}^1. \tag{35}$$

Finally, the writing of the boundary conditions for plane waves at interface I ($x_3 = 0$) leads to 4 equations based on the continuity of the component on the $x_3$-axis of the displacement vector $\mathbf{U}$ and from the continuity of the stress vector $\mathbf{T}$, which is associated with the normal $\mathbf{e}_{x_3}$ to the interfaces, see (14), at interface I (solid 1/fluid 0):

$$U_3^{1(s)}(x_1, x_3 = 0; t) = U_3^{0(s)}(x_1, x_3 = 0; t), \tag{36a}$$

$$\text{and } \mathbf{T}^{1(s)}(x_1, x_3 = 0; t) = \mathbf{T}^{0(s)}(x_1, x_3 = 0; t), \quad \forall x_1, x_3 = 0, \quad \forall t. \tag{36b}$$

It should be noted that, for this scattering problem, the incident field is no longer involved in these equations.

Four unknown amplitudes correspond to these 4 boundary conditions: the amplitude $a_{\text{ref}}^{0(s)}$ of the wave "transmitted" in fluid 0 and the 3 amplitudes ${}^{(\eta)}a^{1(s)}$ ($\eta = 4,5,6$) of the waves "reflected" in solid 1.

These unknown amplitudes can now be determined by solving the linear system of (36).

*3) Solution of the Reflection Problem: Total Reflected Field in Fluid 0:* The scattered displacement field in the fluid (0) is such that

$$\mathbf{u}_{\text{ref}}^{0(s)}(x_1, x_3) = \int_{-\infty}^{+\infty} \left\{ a_{\text{ref}}^{0(s)}(k_1)\, \mathbf{P}_{\text{ref}}^0 \times \exp\left(+ik_3^0 x_3\right) \exp\left(-i\boldsymbol{k}_1 x_1\right) \right\} \mathrm{d}k_1. \tag{37}$$

Finally, the whole reflected field in fluid 0 based on the Kirchhoff approximation is given by (28) in Section II-C-2:

$$\mathbf{u}_{\text{ref}}^{0(k)} = \mathbf{u}_{\text{ref}}^{0(h)} + \mathbf{u}_{\text{ref}}^{0(s)}, \tag{38}$$

where $\mathbf{u}_{\text{ref}}^{0(h)}$ is given by (26) with $(*) = (h)$, and the whole field in fluid 0 can be written as

$$\mathbf{u}^{0(k)} = \mathbf{u}_{\text{inc}}^{0} + \mathbf{u}_{\text{ref}}^{0(k)}. \tag{39}$$

TABLE II. MATERIAL CHARACTERISTICS OF THE UNIDIRECTIONAL CARBON—EPOXY MEDIUM. ELASTIC CONSTANTS (GPA) SUCH THAT 6TH-ORDER AXIS IS PARALLEL TO THE $x_3$-AXIS [51].

| $c_{11}$ | $c_{12}$ | $c_{13}$ | $c_{33}$ | $c_{44}$ | $\rho$ (kg/m$^3$) |
|---|---|---|---|---|---|
| 13.7 | 7.1 | 6.7 | 126 | 5.8 | 1577 |

The reflected pressure $P_{\text{ref}}^{0(*)}$ in fluid 0, corresponding to the problem with a healthy interface II [$(*) = (h)$], an infinite defect on interface II [$(*) = (i)$] or a finite defect [$(*) = (k)$] on interface II under the Kirchhoff approximation is then given by

$$P_{\text{ref}}^{0(*)}(x_1, x_3) = i\omega\rho\, {}^0V\, {}^0 \int_{-\infty}^{+\infty} \left\{ a_{\text{ref}}^{0(*)}(k_1) \times \exp\left(+ik_3^0 x_3\right) \exp\left(-ik_1 x_1\right) \right\} \mathrm{d}\, k_1, \quad (*) = (k),(h),(i), \tag{40a}$$

where

$$a_{\text{ref}}^{0(k)} = a_{\text{ref}}^{0(h)} + a_{\text{ref}}^{0(s)}. \tag{40b}$$

## III. RESULTS FOR CARBON/EPOXY STRUCTURES

Some results obtained on carbon/epoxy structures (see Table II for the elastic constants and the density) are presented in this section, first for a normal incidence ($\theta = 0°$) and various thicknesses (see Section III-A), then when a Lamb mode is excited in the perfectly bonded structure (healthy interface II, see Section III-B-1). In the latter case, the influences of the anisotropy (Section III-B-2), of the length and location of the defect (Sections III-C and III-D), and of the nature of the bonding (Section III-E) are considered.

As far as carbon/epoxy structures are concerned, when the carbon fibers make an angle $\psi$ with the $x_1$-axis, the layer is called a $\psi$-layer. As an example, a 0°/90° structure is made up of the layer 1 with fibers parallel to the $x_1$-axis and of the layer 2 with fibers perpendicular to $x_1$-axis. In the cases considered in this section, the 2 layers have the same thickness ($h_1 = h_2$).

The incident beam is a Gaussian beam and the particle displacement $u_{3\,\text{inc}}^{0E}\left(X_1^E, 0\right)$ in the fluid, normal to the front face of the emitting transducer (see Section II-B-1-a) has the following form

$$u_{3\,\text{inc}}^{0E}\left(X_1^E, 0\right) = U_0 \exp\left[-\left(X_1^E/a\right)^2\right]. \tag{41}$$

The figures present the reflected pressure moduli $P_{\text{ref}}^{0(*)}$ (given by (40) and normalized by the incident pressure) in a plane parallel to the interfaces ($\zeta/a = 1$) as a function of $x_1/a$ (see Fig. 1): a thin solid line is used for an healthy interface II $(*) = (h)$, a dotted line for an infinite defect on interface II $(*) = (i)$, and a thick solid line for a finite-sized defect on interface II $(*) = (k)$. The defect is taken to be a full delamination in Sections III-A, III-B, III-C, and III-D, i.e., the stress vector is equal to zero on the defect, whereas the case of an intermediate (elastic) bonding between solid media 1 and 2 at the interface II is considered in Section III-E.

The frequency is $f = 2$ MHz and the diameter of the transducer is $2a = 20$ mm; subsequently, all the lengths are expressed as multiples of the radius $a$.

### A. Case of Normal Incidence

When $\theta = 0°$ (normal incidence) and when $d = 0$ (defect localized just in front of the transducer), the shape and the amplitude of the reflected fields for an infinite [$(*) = (i)$] or for a finite defect [$(*) = (k)$] on interface II are very similar (some diffraction effects can just be observed for the finite defect case), as can be seen when comparing Figs. 5(a) and (b). For the purpose of nondestructive testing, the amplitudes of the reflected fields for a healthy interface II and for a defect on interface II should be quite different, to provide a good detection of the defect. This is the case for Fig. 5(b) when the product $f.h = 0.2$ MHz·mm but this is no longer the case when the product $f{\cdot}h = 2$ MHz·mm (see Fig. 6): the reflection coefficient in water for plane waves incident on the healthy structure oscillates periodically between 0 and 0.8 as a function of the product frequency by thickness, and thus, if this product is such that the reflection coefficient is close to 0.8, the difference between the reflected fields for a healthy structure and for a structure with a defect (maximum amplitude equal to 1 for a large defect in the case of a delaminating) is too small to provide a good detection of the defect. As a consequence, it seems interesting to study the case of oblique incidence, and especially when the incident beam may generate a Lamb wave into the structure for a given couple (incident angle, frequency).

### B. Case of a Lamb Mode Propagating in the Structure

As far as propagation of Lamb modes in the structure is concerned, the most interesting case for detecting a defect corresponds to the generation of a Lamb mode in the healthy structure (see Sections III-B-1. and III-B-2). When the size of the defect is long enough, the generation of Lamb modes between the upper interface and the defect can also enable the detection and thus be considered. To be more concise, these last results are not reported here.

*1) Case of a Single Isotropic Layer:* The first result for Lamb modes (Fig. 7) concerns the case of identical media constituting layers 1 and 2, which amounts to a defect located in a single 10-mm-thick layer. The fibers are parallel to the $x_2$-axis (one single 90° layer or a 90°/90° structure), which amounts to an isotropic symmetry in the sagittal plane. The inclination of the axis of the incident

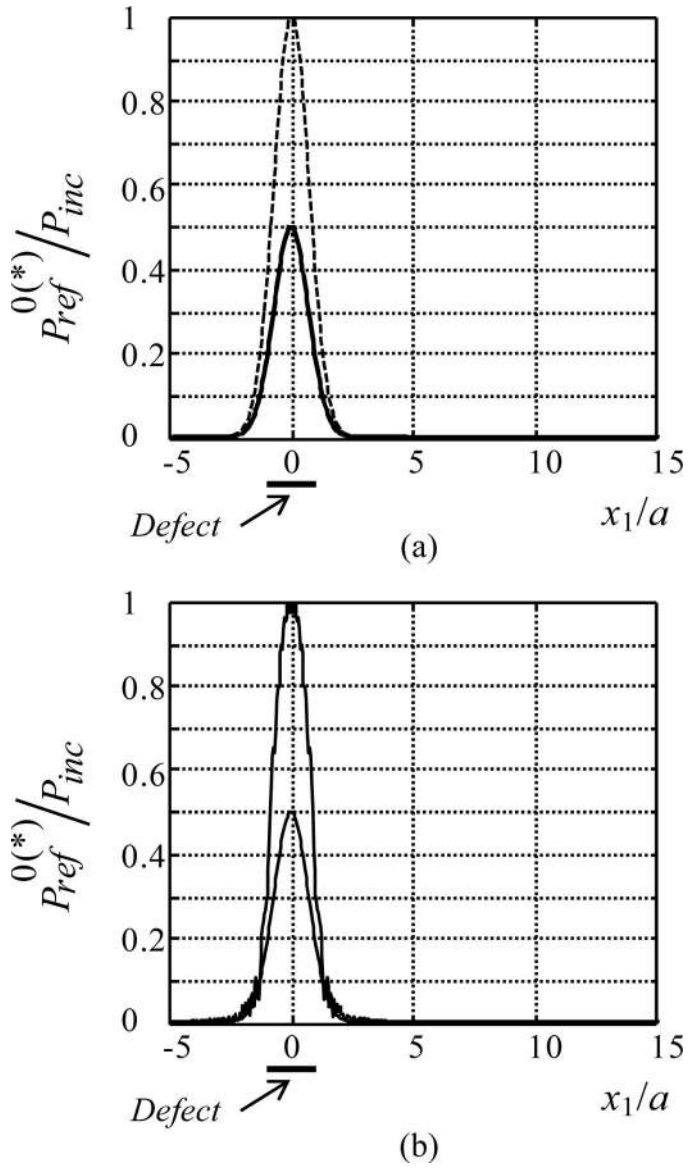


Fig. 5. Reflected pressure $P_{\text{ref}}^{0(*)}$ for a 90°/90° carbon/epoxy structure, $h_1 = h_2 = 0.05$ mm, full delaminating. Thin solid line (*) = ($h$), dotted line (*) = ($i$), and thick solid line (*) = ($k$). Incident angle $\theta = 0°$, frequency $f = 2$ MHz. $\zeta/a = 1$, $d = 0$, $L/a = 1$.

beam is such that a Lamb mode may be generated in the healthy structure, namely, the antisymmetric mode A20 in the case of Fig. 7. The generation of a Lamb mode may be recognized by looking at the reflected pressure $P_{\text{ref}}^{0(h)}$ in the fluid (the thin solid line on Fig. 7) along the cut line at the distance $\zeta$ from the interface I (see Fig. 1). Indeed, a null value of that pressure can be observed between 2 maxima. The first maximum, on the left, corresponds to the specular reflected field on the first interface. The second maximum, on the right, is followed by a slow decreasing of the pressure. This corresponds to the re-emission of the generalized Lamb wave with the well-known associated leaky wave. Because the specular reflected field and the Lamb re-emission field are in phase opposition, this explains the null value of the total pressure in the location where the 2 fields counterbalance each other.

It is important to notice that this interference effect reduces the amplitude of the first maximum (here equal to 0.6 for the normalized pressure), whereas for the same incident angle, the maximum of the reflected pressure $P_{\text{ref}}^{0(i)}$ on the structure with the infinite defect indicated by the dotted line on Fig. 7(a) has its value near 0.9. As expected, the reflected pressure $P_{\text{ref}}^{0(k)}$ for a finite-size defect follows the curve $P_{\text{ref}}^{0(h)}$ outside and far from the defect, as shown in Fig. 7(b), whereas it follows the curve $P_{\text{ref}}^{0(i)}$ in the defect region. Between these regions, the pressure $P_{\text{ref}}^{0(k)}$ presents some scattering effects due to the edges of the defect. As a consequence, the amplitude maximum of the reflected pressure on the structure with the finite defect is here about 1.5 times greater than the amplitude maximum of the reflected pressure on the healthy structure, and we may conclude that this configuration is well suited for a good detection of the defect.

*2) Influence of Anisotropy:* When the fibers in layer 2 are perpendicular to those in layer 1 (a 90°/0° structure), the structure is anisotropic. Starting with the preceding configuration (Section III-B-1), by a progressive rotation around the $x_3$-axis of this second layer, one may follow continuously the Lamb mode A20 to obtain a guided mode for this nonsymmetric structure, which is found to be generated at an incidence of 12.75°.

The corresponding reflected pressures are shown on Fig. 8. The thin line presents the strong trough characteristic of the generation of a guided mode in the healthy structure; as the dotted line for the structure with the infinite defect is very similar to that of Fig. 7(a), it has not been reported on Fig. 8, for clarity. The diffraction parts of the thick line, for the finite defect, are reinforced, compared with that of Fig. 7, due to a greater change of media when passing from layer 1 to layer 2.

A similar case is presented in Fig. 9, for a 0°/90° structure. For the same incident angle, the same guided mode is generated in the structure.

For these 2 cases, the ratio between the maxima of pressure for the healthy structure and for the structure with the finite defect is about 0.4. We may conclude that the generation of this guided mode leads to a good detection of the defect.

The Fig. 10 presents the case of a fully anisotropic structure (30°/120°). The guided mode may be generated for a 12.15° incidence. One observes in this case that the leaky wave presents several maxima that correspond to successive reflections in the structure. The diffraction effects, for the finite defect, are important in this case. Again, this configuration is suitable for good detection of the defect.

### C. Influence of the Length of the Defect

The aim of this section is to show the influence of the length $L$ of the defect on its detectability. The configuration considered for the 90°/0° structure is that of Fig. 8

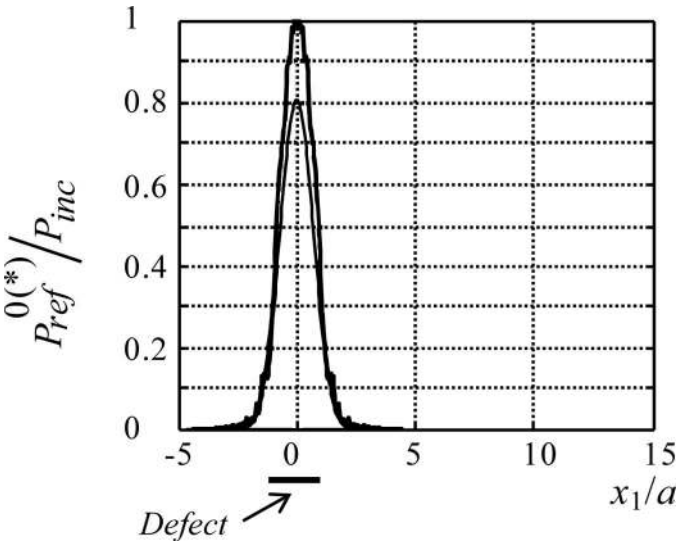


Fig. 6. Reflected pressure $P_{\text{ref}}^{0(*)}$ for a 90°/90° carbon/epoxy structure, $h_1 = h_2 = 5$ mm, full delaminating. Thin solid line (*) = ($h$) and thick solid line (*) = ($k$). Incident angle $\theta = 0°$, frequency $f = 2$ MHz. $\zeta/a = 1$, $d = 0$, $L/a = 1$.

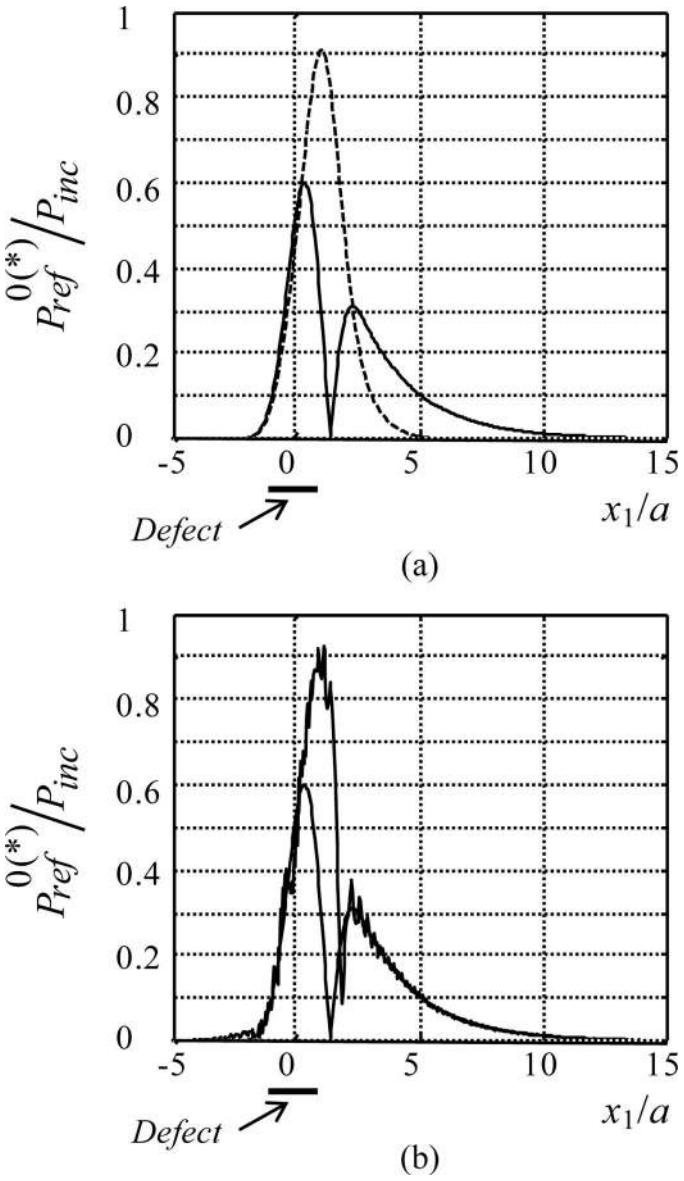


Fig. 7. Reflected pressure $P_{\text{ref}}^{0(*)}$ for a 90°/90° carbon/epoxy structure, $h_1 = h_2 = 5$ mm, full delaminating. Thin solid line (*) = ($h$), dotted line (*) = ($i$), and thick solid line (*) = ($k$). Incident angle $\theta = 11.78°$, frequency $f = 2$ MHz, propagation of an A 20 Lamb mode. $\zeta/a = 1$, $d = 0$, $L/a = 1$.

for $L/a = 1$. Figs. 11 and 12 correspond, respectively, to a length of the defect equal to $2a$ and to $a/10$ ($2a$ is the diameter of the emitter, see Section I).

As expected, the thick solid curve corresponding to the reflected pressure $P_{\text{ref}}^{0(k)}$ (finite-length defect) is closer to the dotted curve corresponding to the reflected pressure $P_{\text{ref}}^{0(i)}$ in Fig. 11 ($L/a = 2$) than in Fig. 8 ($L/a = 1$), but some diffraction effect still exists. In both cases, the defect is well seen but there is more diffraction (especially on the left edge of the defect) when $L/a = 1$ than for a larger defect. This can be explained by the fact that, the greater the length of the defect, the less prominent is the diffraction phenomenon due to the discontinuity of the given (approximate) boundary values on the plane II (see Section II-A-2).

On the other hand, when the length of the defect is much smaller than the radius of the emitter (Fig. 12, $L/a = 0.1$), the reflected pressure $P_{\text{ref}}^{0(k)}$ follows the thin solid curve corresponding to the reflected pressure $P_{\text{ref}}^{0(h)}$ for the healthy structure. Although the presence of the defect generates much diffraction, as can be seen in the thick solid curve for the pressure $P_{\text{ref}}^{0(k)}$, if this curve were smoothed, it would be much too close to the curve for the healthy structure for there to be good detection of the defect.

### *D. Influence of the Location of the Defect*

Figs. 13 and 14 correspond to the same configuration as that of Fig. 8, except that the location of the defect is changed along the interface II: $d = 0$ for Fig. 8, $d = -2a$ for Fig. 13, and $d = 3a$ for Fig. 14 (see Fig. 1 for the geometry and definition of $d$). For clarity, the dotted line corresponding to an infinite defect is not reported on Figs. 13 and 14 (it is the same as that of Fig. 12).

When $d = -2a$, the defect is slightly visible, but the diffraction originating from the right edge of the defect can be distinguished. When $d = 0$, the defect is clearly visible, and the center of the reflected field $P_{\text{ref}}^{0(k)}$ coincides partially with the field $P_{\text{ref}}^{0(i)}$. The diffraction effects originating from the right edge of the defect are well visible. When $d = 3a$, the reflected field $P_{\text{ref}}^{0(k)}$ coincides partially with the field $P_{\text{ref}}^{0(h)}$ for the healthy structure, with diffraction effects coming from the left edge of the defect. However, the detectability of the defect is not so clear.

For larger values of $d$, an artifact of the Kirchhoff approximation would appear. Indeed, the multiple reflections between the upper interface and the infinite defect would lead to values of the re-emission data much greater than

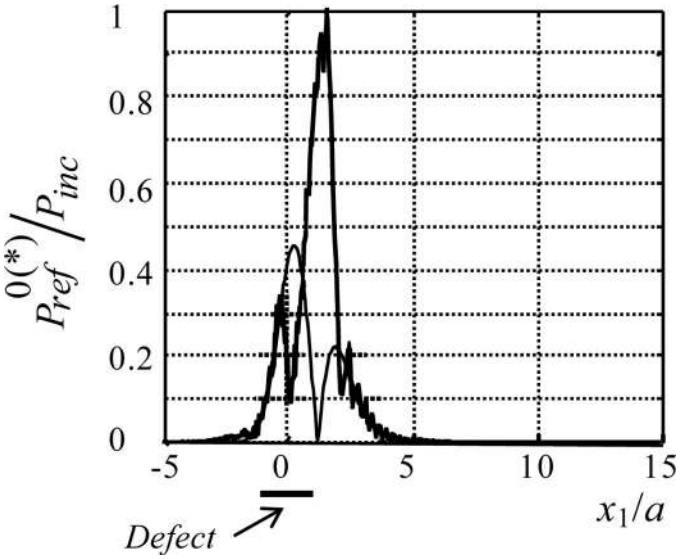


Fig. 8. Reflected pressure $P_{\text{ref}}^{0(*)}$ for a 90°/0° carbon/epoxy structure, $h_1 = h_2 = 5$ mm, full delaminating. Thin solid line (*) = ($h$) and thick solid line (*) = ($k$). Incident angle $\theta = 12.75°$, frequency $f = 2$ MHz, propagation of a Lamb mode. $\zeta/a = 1$, $d = 0$, $L/a = 1$.

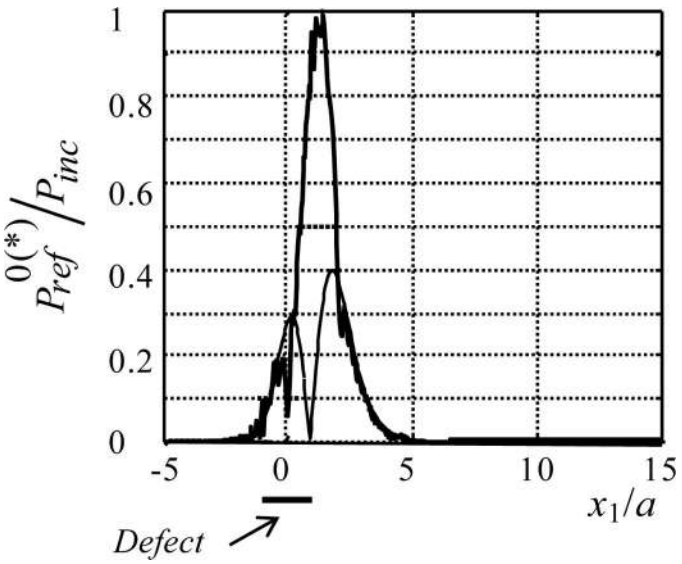


Fig. 9. Reflected pressure $P_{\text{ref}}^{0(*)}$ for a 0°/90° carbon/epoxy structure, $h_1 = h_2 = 5$ mm, full delaminating. Thin solid line (*) = ($h$) and thick solid line (*) = ($k$). Incident angle $\theta = 12.75°$, frequency $f = 2$ MHz, propagation of a Lamb mode. $\zeta/a = 1$, $d = 0$, $L/a = 1$.

they ought to be. To avoid this phenomenon, the Kirchhoff approximation must be implemented in an iterative procedure [52].

### *E. Influence of the Nature of the Bonding*

The section aims to study the influence of the $(3 \times 3)$ matrix $\mathbf{K}$ of stiffness coefficients, defined in Section II-B-3, and involved in boundary conditions (19). The results presented just above correspond to a total delaminating, i.e., to a null matrix $\mathbf{K}$. From a numerical point of view, it appears that a total delaminating corresponds to numerical

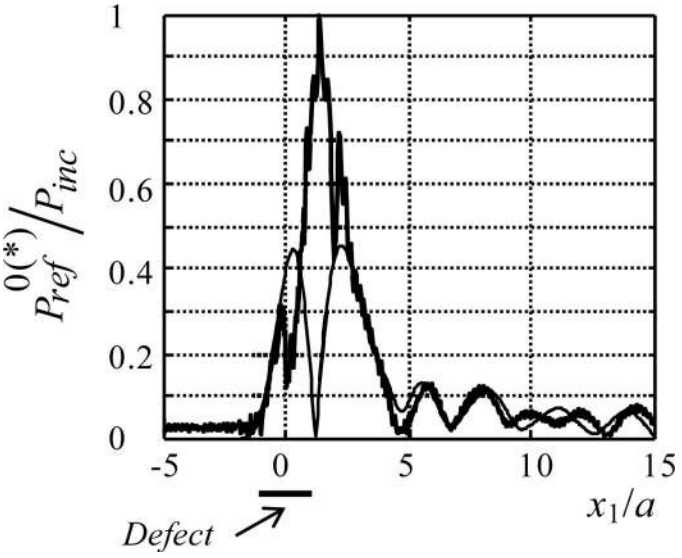


Fig. 10. Reflected pressure $P_{\text{ref}}^{0(*)}$ for a 30°/120° carbon/epoxy structure, $h_1 = h_2 = 5$ mm, full delaminating. Thin solid line (*) = ($h$) and thick solid line (*) = ($k$). Incident angle $\theta = 12.15°$, frequency $f = 2$ MHz, propagation of a Lamb mode. $\zeta/a = 1$, $d = 0$, $L/a = 1$.

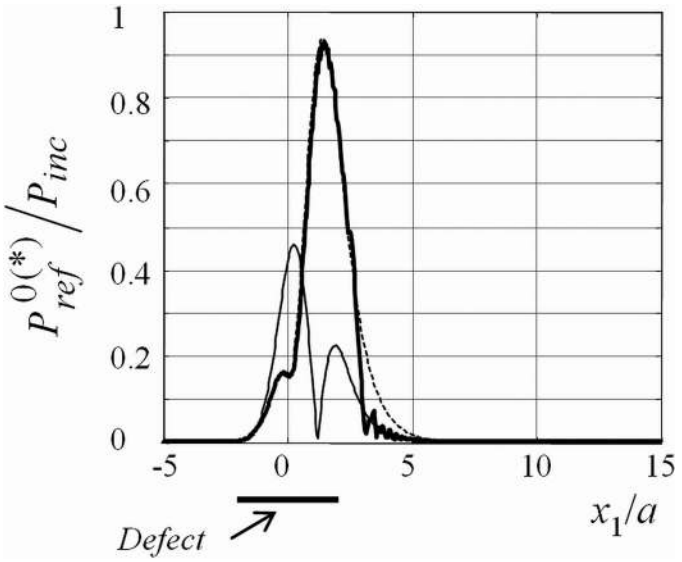


Fig. 11. Reflected pressure $P_{\text{ref}}^{0(*)}$ for a 90°/0° carbon/epoxy structure, $h_1 = h_2 = 5$ mm, full delaminating. Thin solid line (*) = ($h$), dotted line (*) = ($i$), and thick solid line (*) = ($k$). Incident angle $\theta = 12.75°$, frequency $f = 2$ MHz, propagation of a Lamb mode. $\zeta/a = 1$, $d = 0$, $L/a = 2$.

values up to nearly $K_{ii} = 10^{13}\text{N}\cdot\text{m}^{-3}$, see Fig. 15 (Fig. 8 corresponds to $K_{ii} = 5 \times 10^{12}\text{N}\cdot\text{m}^{-3}$). When intermediate (elastic) bonding between the solid media 1 and 2 at the interface II is considered, it can be seen that the defect can still be detected. As expected, the greater the coefficients of the matrix $\mathbf{K}$ (the embedding condition corresponds to infinite coefficients), the less the defect can be detected (see Fig. 16 for $K_{ii} = 3 \times 10^{13}\text{N}\cdot\text{m}^{-3}$) and the weaker the reflected field $P_{\text{ref}}^{0(k)}$. From $K_{ii} = 10^{14}\text{N}\cdot\text{m}^{-3}$, the bonding amounts to a perfect embedding and the curves

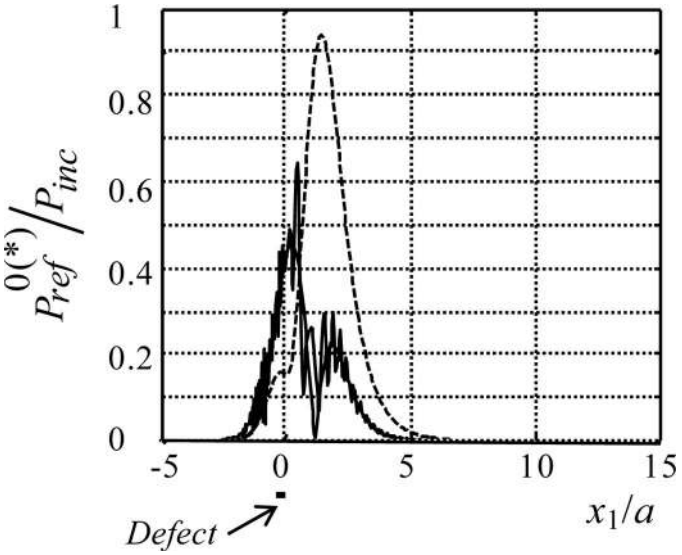


Fig. 12. Reflected pressure $P_{\text{ref}}^{0(*)}$ for a 90°/0° carbon/epoxy structure, $h_1 = h_2 = 5$ mm, full delaminating. Thin solid line (*) = ($h$), dotted line (*) = ($i$), and thick solid line (*) = ($k$). Incident angle $\theta = 12.75°$, frequency $f = 2$ MHz, propagation of a Lamb mode. $\zeta/a = 1$, $d = 0$, $L/a = 0.1$.

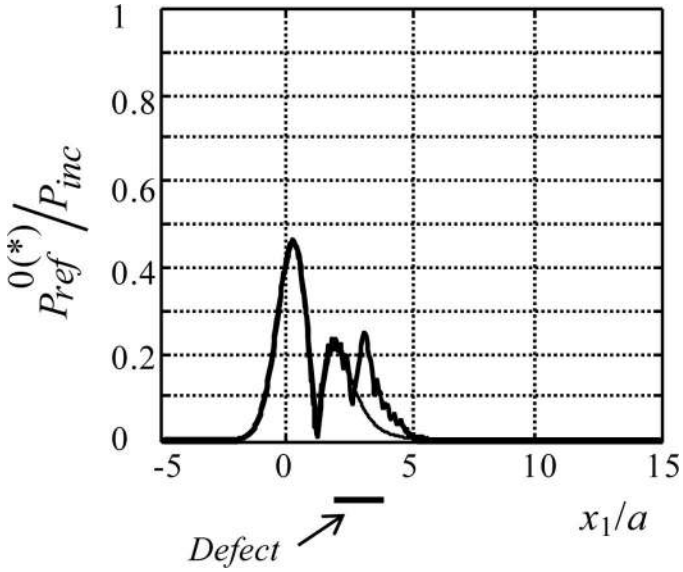


Fig. 14. Reflected pressure $P_{\text{ref}}^{0(*)}$ for a 90°/0° carbon/epoxy structure, $h_1 = h_2 = 5$ mm, full delaminating. Thin solid line (*) = ($h$) and thick solid line (*) = ($k$). Incident angle $\theta = 12.75°$, frequency $f = 2$ MHz, propagation of a Lamb mode. $\zeta/a = 1$, $d = 3a$, $L/a = 1$.

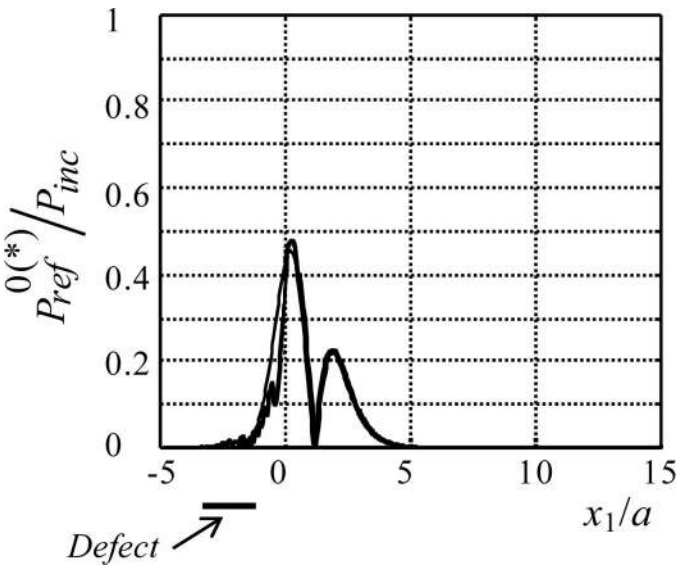


Fig. 13. Reflected pressure $P_{\text{ref}}^{0(*)}$ for a 90°/0° carbon/epoxy structure, $h_1 = h_2 = 5$ mm, full delaminating. Thin solid line (*) = ($h$) and thick solid line (*) = ($k$). Incident angle $\theta = 12.75°$, frequency $f = 2$ MHz, propagation of a Lamb mode. $\zeta/a = 1$, $d = -2a$, $L/a = 1$.

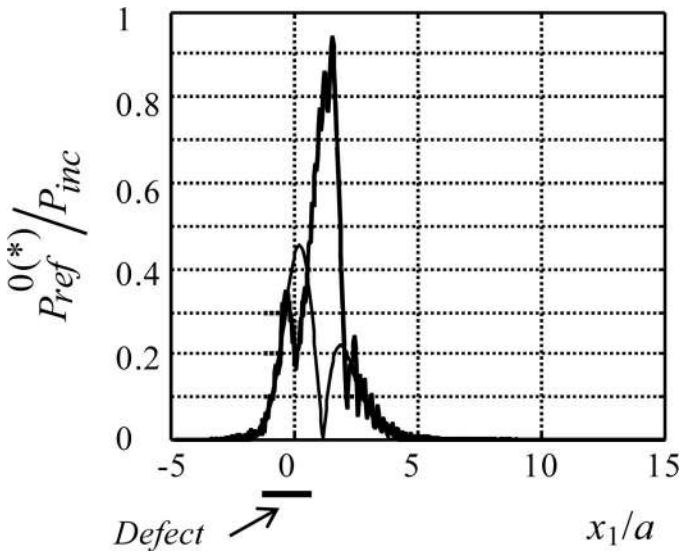


Fig. 15. Reflected pressure $P_{\text{ref}}^{0(*)}$ for a 90°/0° carbon/epoxy structure, $h_1 = h_2 = 5$ mm. Thin solid line (*) = ($h$) and thick solid line (*) = ($k$). Incident angle $\theta = 12.75°$, frequency $f = 2$ MHz, propagation of a Lamb mode. $\zeta/a = 1$, $d = 0$, $L/a = 1$. Coefficients $K_{ii} = 10^{13}\text{N}\cdot\text{m}^{-3}$.

for $P_{\text{ref}}^{0(k)}$ and $P_{\text{ref}}^{0(h)}$ are superimposed. As a consequence, it should be noted that there is a very limited range of values of the defect stiffness coefficients for which ultrasounds will be sensitive to the presence of a bonding defect.

## IV. Conclusion

This paper aimed at providing a semi-analytical model for the interaction of a monochromatic ultrasonic bounded beam with a 2-layered anisotropic structure including a finite defect on the internal interface. Delamination or partial bonding conditions have been assumed on the defect. The scattering of the acoustic field by the defect has been calculated using the Kirchhoff approximation. Plane wave decompositions of the fields, using spatial Fourier transforms, have been used to solve the problem of crossing the various interfaces of the structure (or eventually of a multilayered structure in the case of a general stratified medium) The interaction with the defect has been calculated by introducing a scattered field, which corresponds

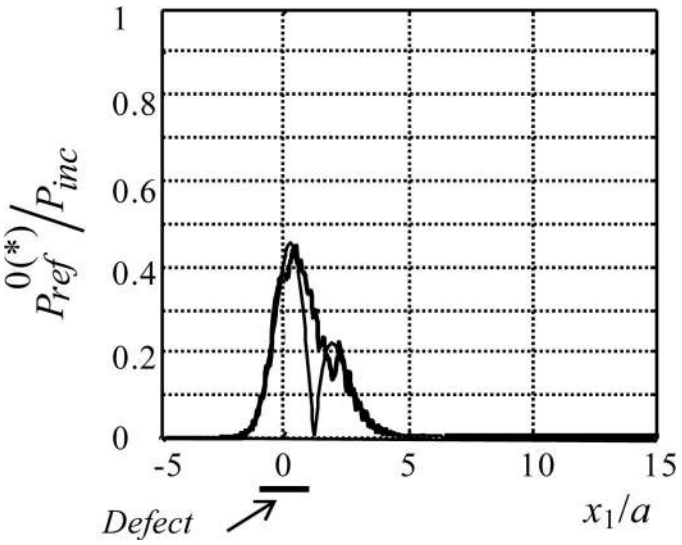


Fig. 16. Reflected pressure $P_{\text{ref}}^{0(*)}$ for a 90°/0° carbon/epoxy structure, $h_1 = h_2 = 5$ mm. Thin solid line $(*) = (h)$ and thick solid line $(*) = (k)$. Incident angle $\theta = 12.75°$, frequency $f = 2$ MHz, propagation of a Lamb mode. $\zeta/a = 1$, $d = 0$, $L/a = 1$. Coefficients $K_{ii} = 3 \times 10^{13}\text{N.m}^{-3}$.

to the perturbation due to the defect, compared with the solution for the healthy structure.

Several results have been presented for the case of a carbon/epoxy composite when the fibers in the 2 layers are parallel or perpendicular. First, it is seen that normal incidence is not always the best configuration to detect clearly the defect. Instead, an incident angle such that a Lamb mode or guided mode can be generated in the healthy structure may be more suitable. The influence of various physical and geometrical parameters on the ability to detect a defect has been studied: length and location of the defect, nature of the glue characteristics for a partial bonding, angle between the beam, and the fibers of the composite.

## References


[1] P. Calmon, S. Mahaut, S. Chatillon, and R. Raillon, "CIVA: An expertise platform for simulation and processing NDT data," *Ultrasonics*, vol. 44, pp. e975–e979, Dec. 2006.

[2] J. D. Achenbach, "Modeling for quantitative non-destructive evaluation," *Ultrasonics*, vol. 40, pp. 1–10, May 2002.

[3] M. J. S. Lowe, "Matrix techniques for modeling ultrasonic waves in multilayered media," *IEEE Trans. Ultrason. Ferroelectr. Freq. Control*, vol. 42, no. 4, pp. 525–542, Jul. 1995.

[4] M. Castaings and B. Hosten, "Delta operator technique to improve the Thomson-Haskell method stability for propagation in multilayered anisotropic absorbing plates," *J. Acoust. Soc. Am.*, vol. 95, no. 4, pp. 1931–1941, 1994.

[5] A. H. Nayfeh, *Wave Propagation in Layered Anisotropic Media with Applications to Composites*, New York: North-Holland, 1995.

[6] C. Potel and J. F. de Belleval, "Acoustic propagation in anisotropic periodically multilayered media; a method to solve numerical instabilities," *J. Appl. Phys.*, vol. 74, no. 4, pp. 2208–2215, 1993.

[7] A. Pilarski, J. L. Rose, and K. Balasubramaniam, "The angular and frequency characteristics of reflectivity from a solid layer embedded between two solids with imperfect boundary conditions," *J. Acoust. Soc. Am.*, vol. 87, no. 2, pp. 532–542, 1990.

[8] M. Spies, "Kirchhoff evaluation of scattered elastic wavefields in anisotropic media," *J. Acoust. Soc. Am.*, vol. 107, pp. 2755–2759, May 2000.

[9] R. Huang, L. W. Schmerr Jr., A. Sedov, and T. A. Gray, "Kirchhoff approximation revisited—Some new results for scattering in isotropic and anisotropic elastic solids," *Res. Nondestr. Eval.*, vol. 17, no. 3, pp. 137–160, 2006.

[10] L. W. Schmerr and S. J. Song, Eds. *Ultrasonic Nondestructive Evaluation Systems: Models and Measurements*, New York: Springer, 1981.

[11] K. G. Foote and D. T. I. Francis, "Comparing Kirchhoff-approximation and boundary-element models for computing gadoid target strengths," *J. Acoust. Soc. Am.*, vol. 111, no. 4, pp. 1644–1654, Apr. 2002.

[12] N. Gengembre and A. Lhémery, "Pencil method in elastodynamics. Application to ultrasonic field computation," *Ultrasonics*, vol. 38, pp. 495–499, Mar. 2000.

[13] R. Croce, P. Calmon, and L. Paradis, "Modeling of propagation and echo formation in a multilayered structure," *Ultrasonics*, vol. 38, pp. 537–541, Mar. 2000.

[14] S. Banerjee and T. Kundu, "Semi-analytical modeling of ultrasonic fields in solids with internal anomalies immersed in a fluid," *Wave Motion*, vol. 45, no. 5, pp. 581–595, 2008.

[15] S. I. Rokhlin, J. Y. Kim, B. Xie, and B. Zoofan, "Nondestructive sizing and localization of internal microcracks in fatigue samples," *NDT&E Int.*, vol. 40, no. 6, pp. 462–470, 2007.

[16] B. Hosten, L. Moreau, and M. Castaings, "Reflection and transmission coefficients for guided waves reflected by defects in viscoelastic material plates," *J. Acoust. Soc. Am.*, vol. 121, no. 6, pp. 3409–3417, Jun. 2007.

[17] J. B. Keller, "Geometrical theory of diffraction," *J. Opt. Soc. Am.*, vol. 52, no. 2, pp. 116–130, Feb. 1962.

[18] J. S. Asvestas and R. E. Kleinman, "The strip," in *Electromagnetic and Acoustic Scattering by Simple Shapes,* rev. ed., J. J. Bowman, T. B. A. Senior, and P. L. E. Uslenghi, Eds. New York: Hemisphere Publishing Corporation, 1987, ch. 4.

[19] A. Gautesen, V. Zernov, and L. Fradkin, "Diffraction coefficients of a semi-infinite planar crack embedded in a transversely isotropic space," *Wave Motion*, vol. 46, no. 1, pp. 29–46, 2009.

[20] N. Bedrici, M. Ben Tahar, Ph. Gatignol, "Interaction d'un faisceau ultrasonore avec un défaut quelconque dans un milieu élastique en présence d'une interface infinie," in 8th Congrès Français d'Acoustique, collected papers on CD-ROM, Apr. 24–27, Tours, France, 2006, pp. 115-118.

[21] N. Bedrici, "Méthode hybride 'Intégrales de Fourier/Eléments finis de frontière' pour l'étude de l'interaction d'un faisceau ultrasonore avec un défaut situé dans un multicouche," Ph.D. dissertation, Univ. Techn. Compiègne, France, 2008.

[22] J. W. Goodman, Ed.*Introduction to Fourier Optics*, New York: McGraw Hill, 1981.

[23] B. Hosten and M. Deschamps, "Transmission ultrasonore en faisceau borné d'une interface plane à l'aide du spectre angulaire d'ondes planes," *Trait. Signal*, vol. 2, no. 1, pp. 195–199, 1985.

[24] M. E. Schaffer, P. A. Lewin, and J. M. Reid, "Propagation through inhomogeneous media using the angular spectrum method," in *Proc. IEEE Trans. Ultrasonics Symp.*, vol. 2, 1987, pp. 943–945.

[25] M. E. Schaffer and P. A. Lewin, "Transducer characterization using the angular spectrum method," *J. Acoust. Soc. Am.*, vol. 85, no. 5, pp. 2204–2214, 1989.

[26] A. Souissi, "Développement des méthodes numériques et expérimentales pour l'étude du champ acoustique de transducteurs ultrasonores en présence d'une interface fluide-solide (réflexion-transmission)," Ph.D. dissertation, Univ. Techn. Compiègne, 1987.

[27] J. F. de Belleval, A. Souissi, P. Gatignol, and N. Mercier, "Modélisation numérique du champ acoustique de transducteurs en présence d'interfaces quelconques ou de milieux multicouches," in *Proc. IXème JESPA*, Marseille, 1990.

[28] D. Orofino and P. Pedersen, "Angle-dependent spectral distortion for an infinite planar fluid-fluid interface," *J. Acoust. Soc. Am.*, vol. 92, pp. 2883–2889, Mar. 1992.

[29] D. Orofino and P. Pedersen, "An angular spectrum technique for calculating receiver output signals for pulse-echo ultrasound insonification of elastics plates," in *Proc. IEEE. Ultrasonics Symp.*, vol. 1, 1992, pp. 667–670.

[30] D. P. Orofino and P. C. Pedersen, "Efficient angular spectrum decomposition of acoustic sources. Part I : Theory," *IEEE Trans. Ultrason. Ferroelectr. Freq. Control*, vol. 40, no. 3, pp. 238–249, May 1993.

[31] D. P. Orofino and P. C. Pedersen, "Efficient angular spectrum decomposition of acoustic sources. Part II: Results," *IEEE Trans. Ul-*

*trason. Ferroelectr. Freq. Control*, vol. 40, no. 3, pp. 250–257, May 1993.
[32] D. Orofino and P. Pedersen, "Evaluation of IP-ASD for elastic media via angular spectrum decomposition," *J. Acoust. Soc. Am.*, vol. 93, no. 3, pp. 1235–1248, 1993.
[33] P. Pedersen and D. Orofino, "Modeling of received ultrasound signals from finite planar targets," *IEEE Trans. Ultrason. Ferroelectr. Freq. Control*, vol. 43, pp. 303–311, Mar. 1996.
[34] S. Zeroug and L. B. Felsen, "Non specular reflection of two- and three-dimensional acoustic beams from fluid-immersed plane-layered elastic structures," *J. Acoust. Soc. Am.*, vol. 95, no. 6, pp. 3075–3089, 1994.
[35] A. U. Rehman, C. Potel, and J. F. de Belleval, "Numerical modeling of the effects on reflected acoustic field for the changes in internal layer orientation of a composite," *Ultrasonics*, vol. 36, no. 1-5, pp. 343–348, 1998.
[36] C. Potel, S. Baly, J. F. De Belleval, M. Lowe, and Ph. Gatignol, "Deviation of a monochromatic Lamb wave beam in anisotropic multilayered media: asymptotic analysis, numerical and experimental results," *IEEE Trans. Ultrason. Ferroelectr. Freq. Control*, vol. 52, no. 6, pp. 987–1001, Jun. 2005.
[37] S. I. Rokhlin, T. K. Bolland, and L. Adler, "Reflection and refraction of elastic waves on a plane interface between two generally anisotropic media," *J. Acoust. Soc. Am.*, vol. 79, no. 4, pp. 3672–3677, 1986.
[38] S. I. Rokhlin, T. K. Bolland, and L. Adler, "Splitting of domain of angles for incident wave vectors in elastic anisotropic media," *J. Appl. Phys.*, vol. 59, no. 11, pp. 3672–3677, 1986.
[39] P. Lanceleur, H. Ribeiro, and J. F. de Belleval, "The use of inhomogeneous waves in the reflection transmission problem at a plane interface between two anisotropic media," *J. Acoust. Soc. Am.*, vol. 93, no. 4, pp. 1882–1892, 1993.
[40] M. Deschamps and C. Changlin, "Réflexion-réfraction de l'onde plane hétérogène: Lois de Snell-Descartes et continuité de l'énergie," *J. Acoust.*, vol. 4, pp. 229–240, 1991.
[41] B. Poirée, "Les ondes planes évanescentes dans les fluides parfaits et les solides élastiques," *J. Acoust.*, vol. 2, pp. 205–221, 1989.
[42] B. A. Auld, Ed., *Acoustic Fields and Waves in Solid*, New York: Wiley, 1973.
[43] D. Royer and E. Dieulesaint, *Elastic Waves in Solids, Vol. 1: Free and Guided Propagation*, Ed. New York: Springer-Verlag, 2000.
[44] E. G. Henneke II, "Reflection-refraction of stress wave at a plane boundary between anisotropic media," *J. Acoust. Soc. Am.*, vol. 51, no. 1B, pp. 210–217, 1972.
[45] L. G. Merkulov, "Ultrasonic waves in crystals," *Appl. Mater. Res*, vol. 2, pp. 231–240, 1963.
[46] M. J. P. Musgrave, *Crystal Acoustics*, San Francisco: Holden-Day, 1970.
[47] J. L. Synge. "Flux of energy for elastic waves in anisotropic media," in *Proc. Royal Irish Academy*, vol. 58, sect. A, Elastic waves in anisotropic media, 1956, pp. 13–21.
[48] J. P. Jones and J. S. Whittier, "Waves at flexibly bonded interface," *J. Appl. Mech.*, vol. 34, pp. 905–908, Dec. 1967.
[49] V. Vlasie and M. Rousseau, "Acoustical validation of the rheological models for a structural bond," *Wave Motion*, vol. 37, no. 4, pp. 333–349, 2003.
[50] E. Levent and J. F. de Belleval "Some results of ultrasonic beam model in anisotropic medium using plane waves decomposition," *Acust.–Acta Acust.*, vol. 82, suppl. 1, pp. S246, 1996.
[51] M. Castaings, "Propagation ultrasonore dans les milieux stratifiés plans constitués de matériaux absorbants et orthotropes," Ph.D. dissertation, Univ. Bordeaux I, 1993.
[52] N. Bedrici, Ph. Gatignol, and C. Potel, "An iterative method for the interaction between a bounded beam and an interface defect in solids, under Kirchhoff approximation," *Acust.–Acta Acust.*, vol. 95, no. 2, pp. 189–202, 2009.

**Bruno Vacossin** is holder of the agrégation in the field of mechanics since 1987. He teaches quality management and nondestructive testing methods at University Picardie Jules Verne in Soissons, France. In 2008, he received a Ph.D. degree in mechanical engineering from the University of Technology of Compiègne (UTC), Compiègne, France, and collaborates with this University in the "Laboratoire Roberval." His research is in the propagation of ultrasonic beams in anisotropic multilayered media, including delaminating defect-type.

**Catherine Potel** received a Ph.D. degree in mechanical engineering from the University of Technology of Compiègne (UTC), Compiègne, France, in 1994. She was lecturer at the University of Amiens, France, from 1996 to 2001 and has been a professor of physical acoustics and of mechanics at the University of Le Mans, France, in the Laboratoire d'Acoustique de l'Université du Maine since 2001. Her research is in ultrasonics for nondestructive evaluation and materials characterization, with special interest in propagation in anisotropic multilayered media such as composites and in rough plates.

**Philippe Gatignol** is holder of the agrégation in the field of mathematics, and he received a Ph.D. degree from the University of Paris VI in 1978. He was lecturer at the University of Paris VI from 1962 to 1981. He was professor of physical acoustics at the University of Technology of Compiègne (UTC), Compiègne, France, from 1981 to 2007 and is now Emeritus Professor. He was project leader at the Scientific Direction of the Sciences for Engineering Department at the National Scientific Research Center (CNRS) and at the French Ministry of Research from 1986 to 1992 and from 1998 to 2000, respectively. He was also responsible for the training of Ph.D. students in mechanics at UTC until 2004. His research is in physical acoustics and ultrasonics for nondestructive evaluation.

**Jean-François de Belleval** (M'87) was born in Marseille, France, in 1944. He received the diploma of engineering at the Ecole Polytechnique, Paris, France, and a Ph.D. degree from the University of Paris VI in 1974 on the subject of the relationship between the acoustic field of a hot jet and its turbulence and infrared emission. He was professor of physical acoustics at the University of Technology of Compiègne (UTC), Compiègne, France, from 1976 to 2004 and is now Emeritus Professor. He was Director of the Laboratoire Roberval, a research unit associated with CNRS from 1992 to 2003. Previously, he worked at ONERA (French Aerospace Research Center). His research is in ultrasonics for nondestructive evaluation and materials characterization, with special interest in propagation in anisotropic multilayered media such as composites.